

On the correct strong-coupling limit in the evolution from BCS superconductivity to Bose-Einstein condensation

P. Pieri and G.C. Strinati

Dipartimento di Matematica e Fisica, Sezione INFM, Università di Camerino, I-62032 Camerino, Italy
e-mail: pieri@str.unicam.it; strinati@camars.unicam.it

(October 14, 1998)

We consider the problem of the crossover from BCS superconductivity to Bose-Einstein condensation in three dimensions for a system of fermions with an attractive interaction, for which we adopt the simplifying assumption of a suitably regularized point-contact interaction. We examine in a critical way the fermionic (self-consistent) T-matrix approximation which has been widely utilized in the literature to describe this crossover *above* the superconducting critical temperature, and show that it fails to yield the correct behaviour of the system in the strong-coupling limit, where composite bosons form as tightly bound fermion pairs. We then set up the correct approximation for a “dilute” system of composite bosons and show that an entire new class of diagrams has to be considered in the place of the fermionic T-matrix approximation for the self-energy. This new class of diagrams correctly describes *both* the weak- and strong-coupling limits, and consequently results into an improved interpolation scheme for the intermediate (crossover) region. In this context, we provide also a systematic mapping between the corresponding diagrammatic theories for the composite bosons and the constituent fermions. As a preliminary result to demonstrate the numerical effect of our new class of diagrams on physical quantities, we calculate the value of the scattering length for composite bosons in the strong-coupling limit and show that it is considerably modified with respect to the result obtained within the self-consistent fermionic T-matrix approximation.

PACS numbers: 74.25.-q, 74.20.-z, 05.30.Jp

I. INTRODUCTION

The problem of the crossover from BCS superconductivity to Bose-Einstein (BE) condensation has attracted considerable interest lately,¹ and especially after the recent ARPES experiments in cuprate superconductors which have shown the existence of a (pseudo) gap at temperatures above the superconducting transition temperature T_c .^{2,3} This observation has prompted the proposal by many authors of the possible presence of quasi-bound fermionic pairs above T_c and up to a second temperature scale T^* . More generally, one may think of ascribing the anomalous experimental properties of the cuprate superconductors in the normal state (i.e., for temperatures T such that $T_c \lesssim T \lesssim T^*$) as well as the possible breakdown of the Fermi-liquid theory to the presence of these quasi-bound pairs.⁴

From the theoretical point of view, this crossover problem (as well as related crossover problems, like the one associated with the Mott transition⁵) poses a compelling challenge, because approximations that are valid on the one side of the crossover are not necessarily valid on the opposite side. In addition, the crossover region is characterized (or even defined) by the absence of a “small” parameter, which would allow one to control the approximations. For systems that are sufficiently “dilute” (such that, for instance, for given strength of the inter-particle interaction, the density ρ can be taken to be arbitrarily small), one could directly exploit the well-known results obtained for “dilute” fermionic systems with $\rho_F = \rho$,

on the one hand,⁶ or for “dilute” bosonic systems with $\rho_B = \rho/2$, on the other hand,⁷ to get a correct description of the limits on the two sides of the crossover.

For a “dilute” fermionic system the two-body equation plays an essential role.⁶ In particular, in three dimensions the low-energy two-body scattering process can be parametrized in terms of the *scattering length* a_F , which is negative for weak coupling and positive for strong coupling (i.e., in the presence of a bound state for the attractive interaction), and diverges when the coupling strength suffices for the bound state to appear. For strong coupling, a_F gives the size of the bound state. The many-body approach to a “dilute” fermionic system then introduces the small dimensionless parameter $k_F a_F$ to select the relevant diagrammatic contributions, whereby the Fermi wave vector identifies the average interparticle distance k_F^{-1} and a_F emerges directly from the many-particle T-matrix (which is defined by repeated scattering in the particle-particle channel at finite fermionic density). In the original treatment with a purely *repulsive* interaction, no bound state occurred and a_F remained finite, in such a way that the parameter $k_F a_F$ could unambiguously be taken to be much less than unity.⁶ In the case of interest to us of an *attractive* interaction, which develops a bound state in three dimensions, however, the parameter $k_F |a_F|$ may readily exceed unity when the strength of the attractive interaction increases toward its critical value for the appearance of a bound state. In this case, the many-body T-matrix can no longer be identified with a_F . Furthermore, past the critical inter-

action strength where the two-body problem develops a bound state (with a_F turning again finite and eventually vanishing in the strong-coupling limit), the many-body T-matrix acquires a singularity (pole) for all interaction strengths and no identification of the T-matrix with a_F is clearly possible any longer. Therefore, although the parameter $k_F a_F$ may still serve to readily locate which side of the crossover one is examining (or even qualitatively, how close to the crossover region one is) by relying on the results of the two-body problem, the smallness of this parameter might not by itself be sufficient to guarantee that an approximation, selected for the weak-coupling limit, is still valid in the strong-coupling limit.

In particular, the T-matrix approximation for the fermionic self-energy (which has invariably been regarded in the literature as representing *the* dilute-approach approximation to the BCS-BE crossover problem)^{8–13} is *not* expected to remain valid as soon as the two-body bound state develops, since for this approximation the power counting in the small parameter $k_F a_F$ relies just on the identification of the many-body T-matrix with a_F . This statement is consistent with the physical picture that, *as soon as the two-body bound state develops, it is the residual interaction between the composite bosons to determine the “diluteness” condition of the system* and not the original attraction between the constituent fermions, which produces the bound state to begin with and relatively to which the system is in the strong-coupling limit.¹⁴ It is then clear that a correct description of the strong-coupling limit can be obtained only by selecting the relevant approximations directly for a *dilute system of composite bosons*, rather than relying on the fermionic T-matrix approximation, which is valid by construction for a *dilute system of fermions*.

From previous work on the functional-integral approach to the crossover from BCS to BE,^{15–17} one knows that approximations (like the BCS mean field at zero temperature), which give a satisfactory account of the weak-coupling limit, become inadequate in the strong-coupling limit, and that only by including fluctuation corrections at least at the one-loop level a sensible description of the effective bosonic system in the strong-coupling limit results. This remark has actually suggested to deal with the crossover problem *in reverse*,¹⁶ that is, by first envisaging approximations which give a satisfactory description of the strong-coupling (bosonic) limit and by extrapolating them toward the weak-coupling (fermionic) limit, where they are expected to work properly as well.¹⁸

One then anticipates the set of many-body (self-energy) diagrams, which describe the bosonic limit, to be much richer than the corresponding set of diagrams, which describe the fermionic limit. In fact, from the previous discussion we do *not* expect the fermionic T-matrix approximation to be appropriate for describing the “dilute” bosonic limit properly. We will indeed show below that the fermionic T-matrix approximation corresponds in the strong-coupling limit to the standard bosonic Hartree-Fock approximation, and that, for this reason,

it misses all but one of the infinite set of self-energy diagrams associated with a “dilute” bosonic system.¹⁹

The dynamics of a “dilute” system of *true* (point-like) bosons can be accounted for by the corresponding T-matrix approximation (aside from a narrow region about T_c).^{7,20,21} Using a representation with a symmetrized two-body interaction, the diagrams corresponding to the bosonic T-matrix approximation contain a sequence of pairs of propagators running in the same direction, with only one additional propagator running in the opposite direction (see Fig. 8b of subsection III-A below). The first term of this sequence (i.e., the one with no pairs but only with the single propagator running backward) corresponds to the standard bosonic Hartree-Fock approximation.¹⁹ Since *all* other terms (with an arbitrary number of pairs running in the same direction) are of the *same order* in the “gas parameter” $\rho_B^{1/3} a_B$ (where a_B is the (positive) scattering length for the low-energy two-boson scattering problem), keeping the Hartree-Fock term only is evidently not justified for a “dilute” bosonic system.

On physical grounds, for a “dilute” system of *composite* bosons (obtained by pairing fermions via the attractive interaction in the strong-coupling limit) one expects the same picture to emerge (as it will also be confirmed by the results of the present paper). For this system, the bosonic single-particle propagator corresponds to a *two-fermion Green’s function* in the particle-particle channel (with opposite spins for a spinless boson), the analogue of the bosonic self-energy corrections being associated in the fermionic particle-particle channel with insertions of the many-body effective interaction. The complete *correspondence* between the two (bosonic and fermionic) diagrammatic structures requires one to establish a well-defined mapping between the building blocks of the two structures (namely, propagators and interaction vertices). One of the purposes of this paper is to discuss this mapping between the two diagrammatic structures, thus complementing the mapping established by means of functional integrals in Ref. 16. It is worth mentioning in this respect that the correspondence we shall find between the *symmetry factors* of the bosonic diagrammatic structure, on the one hand, and the number of independent diagrams in the associated fermionic structure, on the other hand, provides a compelling check on our mapping procedure.

The reason for choosing the particle-particle fermionic channel in order to single out the (approximate) dynamics of the system in the strong-coupling limit stems from the obvious fact that this channel only has *physical relevance* in this limit. The single-particle fermionic propagator (or, equivalently, the fermionic irreducible self-energy) is then obtained as a *derived* quantity, by suitably closing the two-fermion diagrams with a single fermionic line. In this way, the Baym-Kadanoff procedure^{22,23} is effectively inverted, since we construct the one-particle (fermionic) self-energy diagrams in or-

der to recover the *chosen set* of two-particle diagrams via functional differentiation, rather than following the standard procedure of deriving the two-particle diagrams from a chosen set of one-particle diagrams.²⁴

As already mentioned,¹⁴ the interaction between the composite bosons effectively vanishes in the extreme strong-coupling limit. In this *extreme* limit, neither the Hartree-Fock bosonic correction (which results from the standard fermionic T-matrix) nor the set of “low-density” bosonic self-energy diagrams (which are included in the present approach) need then to be taken into account, as they both correspond to interaction corrections. The many-body corrections introduced in this paper in the bosonic limit are thus expected to be important whenever the interaction between the composite bosons has direct influence on physical properties, such as the critical temperature T_c and the bosonic binding energy (pseudogap).¹³ In addition, including the interaction between the composite bosons should make our “low-density” approximation to be valid somewhat closer to the crossover region, over and above the boundary set by retaining the Hartree-Fock term only. In this respect, our finding that the composite-boson scattering length a_B is *smaller* than the value $a_B = 2a_F$ (obtained in Ref. 9 within the fermionic T-matrix approximation) effectively restricts the range of the crossover region on the BE side, and makes the eventual extrapolation of our approximation through the crossover region more reliable.

In this paper, we present the formal theory for the choice of the fermionic self-energy diagrams starting from the strong-coupling side, for temperatures *above* T_c (in the sense that no anomalous single-particle fermionic propagator will be considered) and for three spatial dimensions. The corresponding theory below T_c remains to be developed. An extensive numerical study based on this approximation is under way and will be discussed separately. The only numerical calculation presented in this paper concerns the value of the composite-boson scattering length a_B in the strong-coupling limit.

The plan of the paper is as follows. In Section II we discuss some introductory material, which is necessary for setting up our “low-density” approximation for composite bosons. Specifically: We introduce a suitable regularization for the fermionic point-contact interaction, which allows us to select readily the relevant classes of fermionic diagrams; We summarize the mapping onto a bosonic system in the strong-coupling limit, obtained by the procedure of Ref. 16; We discuss the standard fermionic T-matrix approximation and show how the Hartree-Fock approximation for composite bosons results from it in the strong-coupling limit. In Section III, after recalling the standard theory of the “low-density” Bose gas for true (point-like) bosons, we introduce the theory of the “low-density” Bose gas for composite bosons and obtain the fermionic self-energy from the bosonic self-energy in the “low-density” approximation. In Section IV we present the numerical calculation for the composite-boson scattering length a_B in the strong-coupling limit

and discuss the physical implications of our result. Section V gives our conclusions. The Appendices discuss more technical material. Specifically, in Appendix A we prove that, for our choice of a “contact” fermionic interaction, the composite-boson propagator coincides exactly with the fermionic generalized particle-particle ladder. In Appendix B we discuss in detail the mapping between the bosonic and fermionic diagrammatic structures and demonstrate how the symmetry factors of the bosonic theory translates onto the number of independent diagrams in the fermionic theory, by working out two examples in detail.

II. BUILDING BLOCKS OF THE DIAGRAMMATIC STRUCTURE FOR COMPOSITE BOSONS

In this Section we discuss the diagrammatic structure that generically describes the composite bosons in terms of the constituent fermions, as a preliminary step for setting up the “low-density” approximation for composite bosons in the next Section. Our construction rests on a judicious choice of the fermionic interaction, which (albeit without loss of generality) greatly reduces the number and considerably simplifies the expressions of the Feynman diagrams to be taken into account. We will show how this construction fits with the general mapping established in Ref. 16 via functional-integral methods. We shall, in turn, utilize the results of Ref. 16 to single out the lowest-order (four-point) bosonic vertex as the relevant one in the strong-coupling limit. We shall further show that the standard fermionic T-matrix approximation for a “dilute” Fermi gas^{6,9} reproduces in the strong-coupling limit the Hartree-Fock approximation for composite bosons,¹⁹ which can be defined in analogy with the standard result for true (point-like) bosons.^{20,21} In this way, we shall make manifest the necessity of superseding the standard fermionic T-matrix approximation when dealing with the crossover problem and of replacing it by a more complete approximation, which enables us instead to recover the “low-density” approximation for composite bosons in the strong-coupling limit.

A. Regularization of the fermionic interaction

We begin by considering the following simple model Hamiltonian for interacting fermions (we set Planck \hbar and Boltzmann k_B constants equal to unity throughout):

$$H = \sum_{\sigma} \int d\mathbf{r} \psi_{\sigma}^{\dagger}(\mathbf{r}) \left(-\frac{\nabla^2}{2m} - \mu \right) \psi_{\sigma}(\mathbf{r}) + \frac{1}{2} \sum_{\sigma, \sigma'} \int d\mathbf{r} d\mathbf{r}' \psi_{\sigma}^{\dagger}(\mathbf{r}) \psi_{\sigma'}^{\dagger}(\mathbf{r}') V_{\text{eff}}(\mathbf{r} - \mathbf{r}') \psi_{\sigma'}(\mathbf{r}') \psi_{\sigma}(\mathbf{r}) \quad (2.1)$$

where $\psi_\sigma(\mathbf{r})$ is the fermionic field operator with spin projection $\sigma = (\uparrow, \downarrow)$, m the fermionic (effective) mass, μ the fermionic chemical potential, and $V_{\text{eff}}(\mathbf{r} - \mathbf{r}')$ an *effective potential* that provides the *attraction* between fermions.

To simplify the ensuing many-body diagrammatic structure considerably (and yet preserving the physical effects we are after), we adopt for V_{eff} the simple form of a “contact” potential²⁵

$$V_{\text{eff}}(\mathbf{r} - \mathbf{r}') = v_o \delta(\mathbf{r} - \mathbf{r}') \quad (2.2)$$

where v_o is a negative constant. With this choice, the interaction affects only fermions with opposite spins in the Hamiltonian (2.1) owing to Pauli principle. A suitable *regularization* of the potential (2.2) is, however, required to get accurate control of the many-body diagrammatic structure. In particular, the equation (in the center-of-mass frame)

$$\frac{m}{4\pi a_F} = \frac{1}{v_o} + \int \frac{d\mathbf{k}}{(2\pi)^3} \frac{m}{k^2} \quad (2.3)$$

for the *fermionic scattering length* a_F associated with the potential (2.2) is ill-defined, since the integral over the three-dimensional wave vector \mathbf{k} is ultraviolet divergent. The delta-function potential (2.2) is then effectively regularized, by introducing an ultraviolet cutoff k_o in the integral of Eq. (2.3) and letting $v_o \rightarrow 0$ as $k_o \rightarrow \infty$, in order to keep a_F fixed at a chosen *finite* value. The required relation between v_o and k_o is obtained directly from Eq. (2.3). One finds:

$$v_o = -\frac{2\pi^2}{mk_o} - \frac{\pi^3}{ma_F k_o^2} \quad (2.4)$$

when $k_o|a_F| \gg 1$. Note that a_F enters the expression (2.4) only through the subleading term proportional to k_o^{-2} . Keeping this subleading term turns out to be essential for our purposes. [Note that, if v_o were positive instead of negative, the scattering length a_F would vanish in the limit $k_o \rightarrow \infty$ even keeping v_o finite.]

With the regularization (2.4) for the potential, the classification of the many-body diagrams gets considerably simplified, since only specific sub-structures of these diagrams survive when the limit $k_o \rightarrow \infty$ is eventually taken. Let us consider, in particular, the characteristic rungs occurring in the theory of a “dilute” Fermi gas,⁶ which are depicted in Fig. 1a and Fig. 1b, respectively. For the particle-particle rung of Fig. 1a we obtain:

$$\begin{aligned} I_{pp}(\mathbf{k}_1, \omega_{n_1}; \mathbf{k}_2, \omega_{n_2}) &= \frac{1}{\beta} \sum_{\omega_n} \int \frac{d\mathbf{k}}{(2\pi)^3} v(\mathbf{k}) \\ &\times \mathcal{G}^o(\mathbf{k}_1 + \mathbf{k}, \omega_{n_1} + \omega_n) \mathcal{G}^o(\mathbf{k}_2 - \mathbf{k}, \omega_{n_2} - \omega_n) \\ &= v_o \int \frac{d\mathbf{k}}{(2\pi)^3} \frac{[f_F(\xi(\mathbf{k}_1 + \mathbf{k})) + f_F(\xi(\mathbf{k}_2 - \mathbf{k})) - 1]}{i(\omega_{n_2} + \omega_{n_1}) - \xi(\mathbf{k}_1 + \mathbf{k}) - \xi(\mathbf{k}_2 - \mathbf{k})} \\ &= v_o \left(\frac{mk_o}{2\pi^2} + R_{pp}(\mathbf{k}_1, \omega_{n_1}; \mathbf{k}_2, \omega_{n_2}) \right) \end{aligned} \quad (2.5)$$

where β is the inverse temperature, $\omega_n = (2n + 1)\pi\beta^{-1}$ (n integer) a fermionic Matsubara frequency, \mathcal{G}^o a (bare) single-particle fermionic Green’s function, $f_F(E) = (e^{\beta E} + 1)^{-1}$ the Fermi function, $\xi(\mathbf{k}) = \mathbf{k}^2/(2m) - \mu$, and R_{pp} is a remainder that converges to a finite value in the limit $k_o \rightarrow \infty$. Note that $I_{pp} = -1 + \mathcal{O}(k_o^{-1})$ owing to Eq. (2.4).

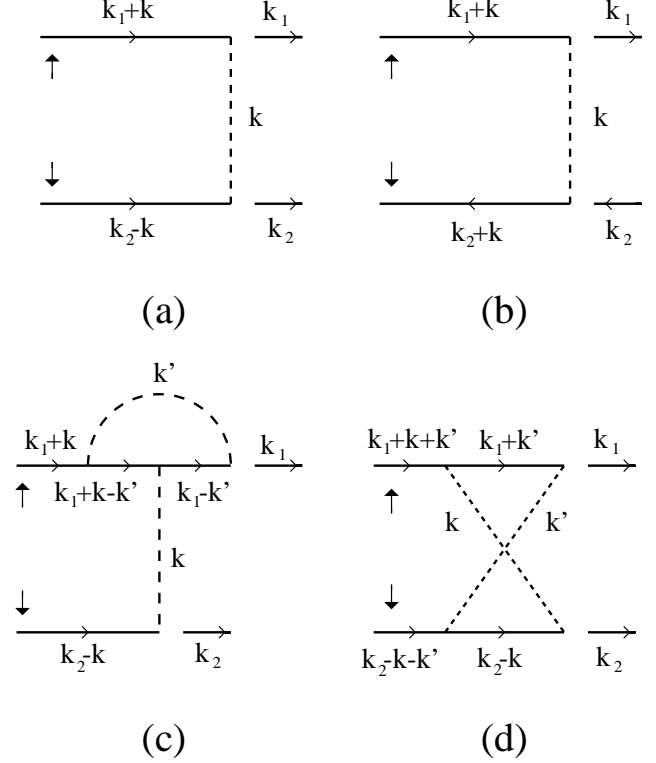


FIG. 1. (a) Particle-particle and (b) particle-hole rung; (c) vertex correction and (d) two-particle effective interaction. Full and broken lines represent the “bare” single-particle fermionic Green’s function and the fermionic interaction, respectively. Four-momenta are indicated and spin labels are represented by up and down arrows.

By the same token, for the particle-hole rung of Fig. 1b we obtain:

$$\begin{aligned} I_{ph}(\mathbf{k}_1, \omega_{n_1}; \mathbf{k}_2, \omega_{n_2}) &= \frac{1}{\beta} \sum_{\omega_n} \int \frac{d\mathbf{k}}{(2\pi)^3} v(\mathbf{k}) \\ &\times \mathcal{G}^o(\mathbf{k}_1 + \mathbf{k}, \omega_{n_1} + \omega_n) \mathcal{G}^o(\mathbf{k}_2 + \mathbf{k}, \omega_{n_2} + \omega_n) \\ &= v_o \int \frac{d\mathbf{k}}{(2\pi)^3} \frac{[f_F(\xi(\mathbf{k}_1 + \mathbf{k})) - f_F(\xi(\mathbf{k}_2 + \mathbf{k}))]}{i(\omega_{n_2} - \omega_{n_1}) + \xi(\mathbf{k}_1 + \mathbf{k}) - \xi(\mathbf{k}_2 + \mathbf{k})} \end{aligned} \quad (2.6)$$

which vanishes in the limit $k_o \rightarrow \infty$ owing to the vanishing of the prefactor v_o . In this case, the integral over \mathbf{k} on the right-hand side of Eq. (2.6) remains finite in the limit, because $f_F(\xi(\mathbf{k}))$ is proportional to $\exp\{-\beta \mathbf{k}^2/(2m)\}$ for large $|\mathbf{k}|$ (irrespective of the value of the chemical potential). This situation has to be contrasted with the original argument by Galitskii, whereby for a finite-range potential the particle-hole rung I_{ph} does not vanish, but

it is reduced with respect to its particle-particle counterpart I_{pp} by a factor $k_F a_F$ (k_F being the Fermi wave vector).⁶ In the weak-coupling limit, in fact, the integral on the right-hand side of Eq. (2.6) is proportional to k_F from dimensional considerations.

In an analogous way, one can show that in the particle-particle channel the contributions of the vertex corrections (like the one depicted in Fig. 1c) and of the two-particle effective interactions other than the rung (like the one depicted in Fig. 1d) vanish for our choice of the potential, since they both contain a factor I_{ph} of the particle-hole type. [Note that the diagram of Fig. 1c contains also a forbidden interaction between parallel spins.]

Despite these drastic simplifications, care should be exerted in not dismissing too promptly contributions which, albeit being individually vanishing as $k_o \rightarrow \infty$, belong to an infinite sequence that could instead converge to a finite value. Two examples of alternative behaviors are given in Fig. 2a and Fig. 2b. In particular, for the particle-particle ladder of Fig. 2a we obtain from Eq. (2.5) (apart from an overall minus sign originating from the fermionic diagrammatic rules) :

$$\begin{aligned} & \frac{v_o}{1 + I_{pp}(k_1, k_2)} \\ &= - \frac{\frac{2\pi^2}{mk_o} + \frac{\pi^3}{ma_F k_o^2}}{1 - \left(\frac{2\pi^2}{mk_o} + \frac{\pi^3}{ma_F k_o^2} \right) \left(\frac{mk_o}{2\pi^2} + R_{pp}(k_1 + k_2) \right)} \\ &= \frac{1}{\frac{m}{4\pi a_F} + R_{pp}(k_1 + k_2)} \end{aligned} \quad (2.7)$$

since both numerator and denominator in Eq. (2.7) vanish like k_o^{-1} when $k_o \rightarrow \infty$. [Note that we have introduced the four-vector notation $k \equiv (\mathbf{k}, \omega_n)$. Note also that we have attached the \uparrow spin to the upper line and the \downarrow spin to the lower line of the ladder, respectively. This convention will be consistently maintained in the following.] For the particle-hole bubble series of Fig. 2b we obtain instead a vanishing result, since

$$\frac{v_o}{1 + I_{ph}(q; 0)} \rightarrow 0 \quad (2.8)$$

as $k_o \rightarrow \infty$.²⁶

The particle-particle ladder (2.7), upon surviving the limit $k_o \rightarrow \infty$, represents a building block of the many-body diagrammatic structure. It is thus relevant to examine in detail its analytic behavior in the weak- and strong-coupling limits, in the order. Let

$$E_\alpha = i(\omega_{n_1} + \omega_{n_2}) - \frac{(\mathbf{k}_1 + \mathbf{k}_2)^2}{4m} + 2\mu \quad (2.9)$$

be the (complex) energy entering the denominator in Eq. (2.5) and $k_\alpha = \sqrt{2mE_\alpha}$ the associated (complex) wave vector. In the weak-coupling limit,²⁷ both the f_F terms and the -1 term within brackets in Eq. (2.5) contribute to R_{pp} , yielding contributions proportional to k_F

and k_α , respectively. One then obtains the following *finite result* for the particle-particle ladder (2.7)

$$\begin{aligned} & \frac{1}{\frac{m}{4\pi a_F} + R_{pp}(k_1 + k_2)} \\ & \cong \frac{4\pi a_F}{m} \left(1 + \mathcal{O}(k_F a_F) + \mathcal{O}(k_\alpha a_F) \right), \end{aligned} \quad (2.10)$$

which permits one to classify the diagrammatic structure in powers of $k_F a_F$ (and/or of $k_\alpha a_F$) in the weak-coupling limit.⁶

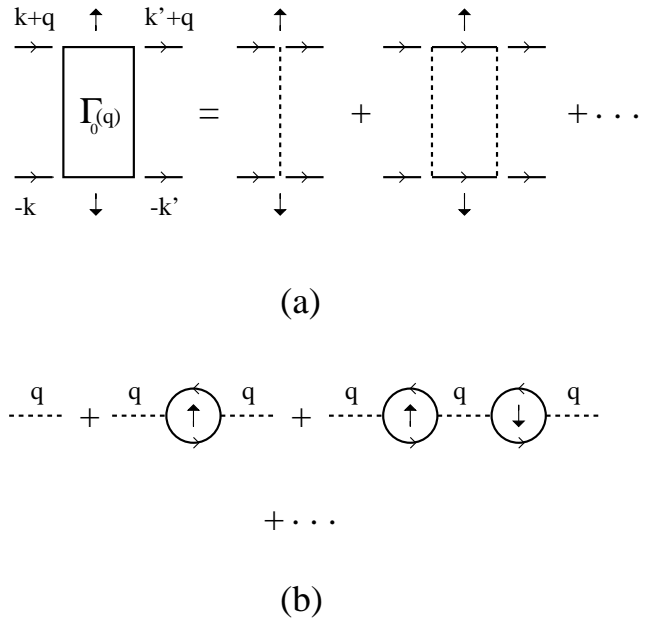


FIG. 2. (a) Particle-particle ladder and (b) series of particle-hole bubbles. Note that for a point-contact potential the particle-particle ladder depends only on the sum of the incoming (outgoing) four-momenta. Conventions are as in Fig. 1.

In the strong-coupling limit (whereby $\beta\mu \rightarrow -\infty$),²⁷ on the other hand, only the -1 term within brackets in Eq. (2.5) contributes to R_{pp} , yielding

$$R_{pp}(k_1 + k_2) = i \frac{m^{3/2}}{4\pi} \sqrt{E_\alpha} \text{sgn}(\text{Im} E_\alpha) \quad (2.11)$$

with the standard convention for the cut of the square root along the negative real axis. Recalling further that $2|\mu| = (ma_F^2)^{-1}$ in the (extreme) strong-coupling limit,¹⁶ we obtain for the particle-particle ladder (2.7) the following *polar structure*

$$\frac{1}{\frac{m}{4\pi a_F} + R_{pp}(k_1 + k_2)} \cong \frac{8\pi}{m^2 a_F} \frac{1}{i(\omega_{n_1} + \omega_{n_2}) - \frac{(\mathbf{k}_1 + \mathbf{k}_2)^2}{4m}} \quad (2.12)$$

which (apart from the residue being different from unity) resembles a “free” boson propagator with Matsubara frequency $\Omega_\nu = \omega_{n_1} + \omega_{n_2} = 2\nu\pi\beta^{-1}$ (ν integer), wave

vector $\mathbf{q} = \mathbf{k}_1 + \mathbf{k}_2$, mass $2m$, and vanishing chemical potential. [More generally, the bosonic chemical potential $\mu_B = 2\mu + \epsilon_o$ should be added to the denominator of Eq. (2.12), where ϵ_o is the bound-state energy of the two-fermion problem - cf. subsection IIIB. In the extreme strong-coupling limit μ_B vanishes.] The complete analogy between the fermionic generalized particle-particle ladder (of which the “bare” particle-particle ladder (2.7) is only a piece) and the “full” boson propagator is discussed in Appendix A.

It is evident from the above considerations that the classification of diagrams developed for a “dilute” system in weak coupling (which relies on the finite value (2.10) of the particle-particle ladder - cf. Ref. 6) can no longer be utilized in the strong-coupling limit, since in this case the particle-particle ladder does not reduce to a constant but develops a polar structure [cf. Eq. (2.12)]. *In the strong-coupling limit, a different classification scheme is therefore required to organize the diagrammatic structure for a “dilute” system.*

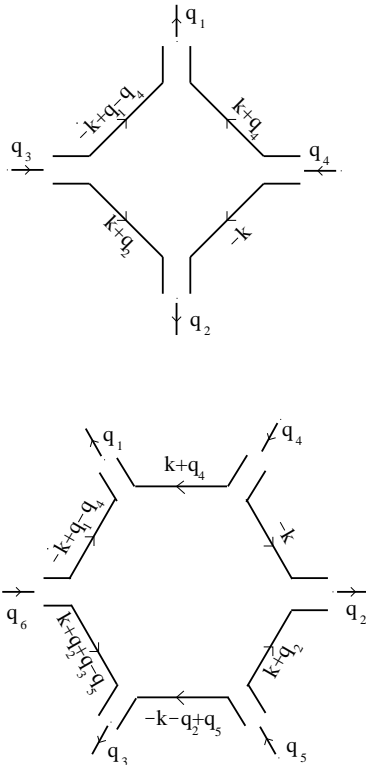


FIG. 3. Four- and six-point vertices for composite bosons. Incoming and outgoing bosonic four-momenta are indicated, as well as four-momenta on each fermionic line. Spin labels are understood to alternate on successive fermionic lines.

It is also evident from the above considerations that, with our choice of the fermionic interaction, the *skeleton structure* of the diagrammatic theory can be constructed only with the particle-particle ladder (2.7) plus an infinite number of interaction vertices, like the ones depicted in Fig. 3 (besides *one* spare single-particle fermionic Green’s

function that enters the fermionic self-energy diagrams, which in turn contains in principle all self-energy insertions originating from self-consistency).

The ladder and the vertices of Fig. 3 contain, by construction, only “bare” single-particle fermionic Green’s functions. These vertices serve to connect the ladders among themselves, thus generating complex diagrammatic structures. In analogy with the so-called Hikami vertices occurring in the weak-localization problem,²⁸ we refer to these vertices as the four, six, ..., -point vertices, in the order.

As far as the dressing of the particle-particle ladder is concerned, the above statements can be justified in a rigorous fashion by resorting, e.g., to functional-integral methods. To this end, in the following subsection we recall some relevant results obtained in Ref. 16, adapting them to the purposes of the present paper.

B. Mapping onto a bosonic system via functional integrals

We briefly review the procedure of Ref. 16 to extract the set of effective bosonic interactions mentioned above from the original fermionic action. We first note that comparison with the results of Ref. 16 requires us to interpret the Fourier transform of the effective attractive potential in Eq. (2.1) as a “separable” potential, of the form

$$\frac{1}{\mathcal{V}} V_{\text{eff}}(\mathbf{k} - \mathbf{k}') \longrightarrow V w(\mathbf{k}) w(\mathbf{k}') \quad (2.13)$$

where \mathcal{V} is the quantization volume, V is a negative constant, and

$$w(\mathbf{k}) = \begin{cases} 1 & \text{if } |\mathbf{k}| < k_o \\ 0 & \text{otherwise} \end{cases}.$$

Note that the limit $k_o \rightarrow \infty$ recovers our “contact” potential, provided we identify $V = v_o/\mathcal{V}$, with v_o given by (2.4).

In Ref. 16 the original fermionic partition function was written in the form of a functional integral

$$\mathcal{Z} = \int \mathcal{D}\bar{c}\mathcal{D}c \exp\{-S\} \quad (2.14)$$

with action

$$S = \int_0^\beta d\tau \left(\sum_{\mathbf{k}, \sigma} \bar{c}_\sigma(\mathbf{k}, \tau) \frac{\partial}{\partial \tau} c_\sigma(\mathbf{k}, \tau) + H(\tau) \right), \quad (2.15)$$

where τ is the imaginary time and (c, \bar{c}) are Grassmann variables. Owing to the form (2.13) of the interaction potential, the quartic part of the Hamiltonian was further expressed in terms of the operator

$$\mathcal{B}(\mathbf{q}, \tau) = \sum_{\mathbf{k}} w(\mathbf{k}) c_{\downarrow}(-\mathbf{k} + \mathbf{q}/2, \tau) c_{\uparrow}(\mathbf{k} + \mathbf{q}/2, \tau) . \quad (2.16)$$

With the use of the following Hubbard-Stratonovich transformation (in the particle-particle channel)

$$\exp \{ -V \bar{\mathcal{B}}(\mathbf{q}, \tau) \mathcal{B}(\mathbf{q}, \tau) \} = -\frac{1}{\pi V} \int db^*(\mathbf{q}, \tau) db(\mathbf{q}, \tau) \quad (2.17)$$

$$\times \exp \left\{ \frac{1}{V} |b(\mathbf{q}, \tau)|^2 + b(\mathbf{q}, \tau) \bar{\mathcal{B}}(\mathbf{q}, \tau) + b^*(\mathbf{q}, \tau) \mathcal{B}(\mathbf{q}, \tau) \right\}$$

where $b(\mathbf{q}, \tau + \beta) = b(\mathbf{q}, \tau)$ for any \mathbf{q} and τ , the Grassmann variables were eventually integrated out, to obtain (apart from irrelevant numerical constants)

$$\mathcal{Z} = \int \mathcal{D}b^* \mathcal{D}b \exp \{ -S_{\text{eff}} \} \quad (2.18)$$

with the “effective” bosonic action

$$S_{\text{eff}} = -\frac{1}{\beta V} \sum_q |b(q)|^2 - \text{tr} \ln \mathbf{M} . \quad (2.19)$$

In Eq. (2.19), we have set $q \equiv (\mathbf{q}, \Omega_\nu)$, the matrix \mathbf{M} is given by

$$\mathbf{M}(k, k') = \begin{pmatrix} \epsilon(k) \delta_{k, k'} & , & \frac{1}{\beta} w(\frac{k+k'}{2}) b^*(k-k') \\ \frac{1}{\beta} w(\frac{k+k'}{2}) b(k'-k) & , & -\epsilon(-k) \delta_{k, k'} \end{pmatrix} \quad (2.20)$$

with $\epsilon(k) = i\omega_n - \xi(\mathbf{k})$, and the trace is over the four-momentum and the matrix indices. The *effective* action S_{eff} contains *all powers* in the bosonic-like variables b . Expanding the logarithm in Eq. (2.19) in fact yields

$$S_{\text{eff}} = -\text{tr} \ln \mathbf{M}_S - \frac{1}{\beta V} \sum_q |b(q)|^2 + \sum_{l=1}^{\infty} \frac{1}{2l} \text{tr} X^{2l} \quad (2.21)$$

where

$$\mathbf{M}_S(k, k') = \begin{pmatrix} \epsilon(k) & 0 \\ 0 & -\epsilon(-k) \end{pmatrix} \delta_{k, k'} \quad (2.22)$$

and

$$X(k, k') = w \left(\frac{k+k'}{2} \right) \begin{pmatrix} 0 & \frac{b^*(k-k')}{\beta \epsilon(k)} \\ -\frac{b(k'-k)}{\beta \epsilon(-k)} & 0 \end{pmatrix} . \quad (2.23)$$

Consider the *quadratic* terms first. The ensuing quadratic action reads:

$$S_{\text{eff}}^{(2)} = \frac{1}{\beta^2} \sum_q |b(q)|^2 A(q) \quad (2.24)$$

where

$$A(q) = -\frac{\beta}{V} - \beta \sum_{\mathbf{k}} w^2(\mathbf{k} - \mathbf{q}/2) \frac{[f_F(\xi(\mathbf{k})) + f_F(\xi(\mathbf{k} - \mathbf{q})) - 1]}{i\Omega_\nu - \xi(\mathbf{k}) - \xi(\mathbf{k} - \mathbf{q})}$$

$$= -\frac{\beta}{V} \left(1 + I_{pp}(q) \right) \quad (2.25)$$

with I_{pp} given by Eq. (2.5). The “bare” bosonic propagator is thus expressed in terms of the particle-particle ladder (2.7), by writing

$$\langle b^*(q) b(q) \rangle_{S_{\text{eff}}^{(2)}} = -\frac{\beta}{V} \frac{v_o}{1 + I_{pp}(q)} \equiv \frac{\beta}{V} \Gamma_o(q) \quad (2.26)$$

where $\Gamma_o(q)$ is the particle-particle ladder depicted in Fig. 2a (including now the appropriate overall sign that was missing in Eq. (2.7)). This identification is shown graphically in Fig. 4a for a definite choice of the spin labels (this convention will be maintained in the rest of the paper). Note that the factor β/V of Eq. (2.26) enters also the definition of the “full” bosonic propagator discussed in Appendix A.

It is important to emphasize that the identification (2.26) (as well as the other results of this subsection and of Appendix A) holds *irrespective* of the value of the fermionic scattering length a_F . Nonetheless, referring to a system of interacting composite bosons acquires physical meaning in the strong-coupling limit only.

For the *quartic* terms we obtain instead from Eq. (2.21)

$$S_{\text{eff}}^{(4)} = \frac{1}{4} \text{tr} X^4 = \frac{1}{4\beta V} \sum_{q_1 \dots q_4} \tilde{u}_2(q_1 \dots q_4) b^*(q_1) b^*(q_2) b(q_3) b(q_4) \quad (2.27)$$

where the (four-point) *effective two-boson interaction* is given by [cf. Fig. 3]

$$\tilde{u}_2(q_1 \dots q_4) = \delta_{q_1+q_2, q_3+q_4} \left(\frac{V}{\beta} \right)^2 \frac{2}{\beta V}$$

$$\times \sum_k \frac{1}{\epsilon(-k) \epsilon(k+q_2) \epsilon(-k+q_1-q_4) \epsilon(k+q_4)} \quad (2.28)$$

with the limit $k_o \rightarrow \infty$ already taken in the last expression. It is worth noting the following features of the above expressions: (i) The factor 1/4 (instead of 1/2) in Eq. (2.27) applies to a *symmetrized* bosonic two-body interaction, which makes the counting of the bosonic Feynman diagrams easier^{20,21}; (ii) The interaction (2.28) is indeed symmetric under the interchange $q_1 \leftrightarrow q_2$ or $q_3 \leftrightarrow q_4$, as it can be explicitly verified; (iii) The interaction (2.28) depends on wave vectors *as well as* on Matsubara frequencies, revealing in this way the composite nature of the bosons; (iv) The factors β and V entering Eqs. (2.27) and (2.28) are needed to comply with the standard bosonic and fermionic diagrammatic rules and with the definition of the “full” bosonic propagator given in Appendix A; (v) The energy denominators in

Eq. (2.28) correspond to single-particle (bare) fermionic Green's functions, since $\mathcal{G}^o(k) = \epsilon(k)^{-1}$; (vi) The factor of 2 in the definition (2.28) corresponds to the two different sequences of spin labels that can be attached to the four fermionic Green's functions, as shown graphically in Fig. 4b (where the identification with the effective two-boson interaction is also indicated). Keeping track of the spin labels will, in fact, prove important in the following to establish the desired mapping between the bosonic and fermionic diagrammatic structures.

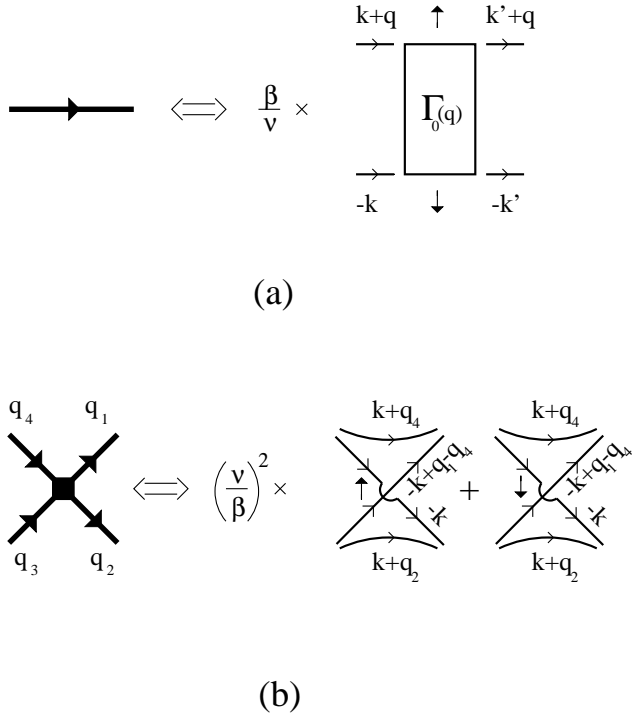


FIG. 4. Graphical correspondence (a) between the “bare” propagator for composite bosons (represented by a thick line) and the fermionic particle-particle ladder of Fig. 2a, and (b) between the effective two-boson interaction and the four-point vertex of Fig. 3, where now the spin labels have been explicitly indicated in the internal lines. Note that the fermionic lines composing the four-point vertex have been rearranged with respect to Fig. 3, in order to resemble the bosonic vertex more closely (accordingly, the fermionic lines never intersect each other in the four-point vertex). Appropriate powers of β/\mathcal{V} as required by Eqs. (2.26) and (2.28) have been indicated explicitly.

When considering the sum $S_{\text{eff}}^{(2)} + S_{\text{eff}}^{(4)}$ of the quadratic and quartic actions, the bosonic propagator $< b^*(q)b(q) >_{S_{\text{eff}}^{(2)} + S_{\text{eff}}^{(4)}}$ can be expressed in terms of the “bare” bosonic propagator (2.26) and of the effective two-boson interaction (2.28) via Wick’s theorem. The topology of the resulting diagrammatic structure, as well as the symmetry factor of each diagram, are identical to those obtained for true (point-like) bosons.^{20,21} The associated fermionic diagrammatic structure can then be constructed whenever needed by the correspondence rules

shown in Fig. 4.

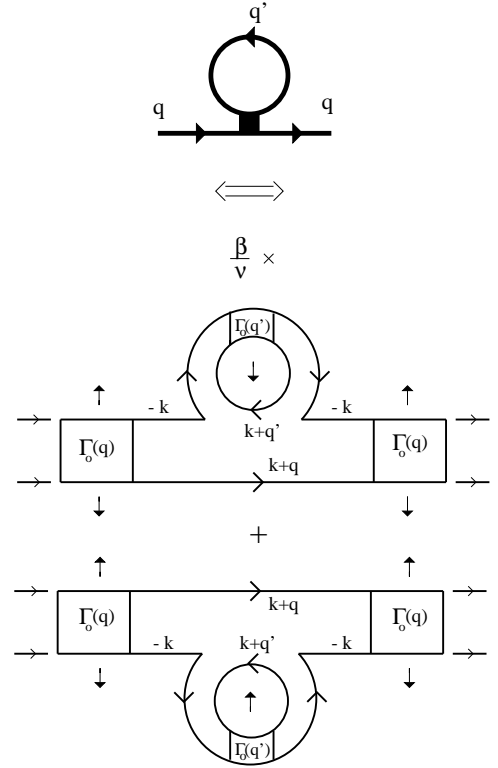


FIG. 5. Graphical correspondence between the composite-boson propagator and the two-fermion Green’s function in the particle-particle channel, to first order in the *four-point* interaction vertex. This vertex can be identified from Fig. 3 by setting $q_2 = q_3 = q$ and $q_1 = q_4 = q'$ therein.

As an example of this correspondence, we show in Fig. 5 the bosonic propagator to first order in the interaction, together with the associated fermionic diagrams for the two-fermion Green’s function in the particle-particle channel. Since the symmetry factor of this bosonic diagram is unity, only two fermionic diagrams are associated with it. [The value of the bosonic symmetry factor and the number of independent fermionic diagrams are intimately connected, as it will be discussed in Appendix B.] Note that a factor $1/(\beta\mathcal{V})$ is attached to the sum over q' in both bosonic and fermionic diagrams. Note also that the minus sign, which is associated with one power of the interaction in the bosonic diagram, is associated instead with the presence of a closed loop in the corresponding fermionic diagrams (the minus signs associated with the fermionic interaction being already taken into account in the definition of the particle-particle ladder). Note finally that the bosonic self-energy insertion of Fig. 5 has the same topological structure of the bosonic Hartree-Fock self-energy diagram.^{20,21}

A typical value of the two-boson effective interaction is obtained by considering the strong-coupling limit $\beta\mu \rightarrow -\infty$ and setting $q_1 = \dots = q_4 = 0$ in Eq. (2.28). One gets:

$$\tilde{u}_2(0) = 2 \left(\frac{\mathcal{V}}{\beta} \right)^2 \left(\frac{m^2 a_F}{8\pi} \right)^2 u_2(0) \quad (2.29)$$

where¹⁶

$$u_2(0) = \frac{4\pi(2a_F)}{2m}. \quad (2.30)$$

The factor $m^2 a_F / (8\pi)$ in Eq. (2.29) reflects the difference between the true bosonic propagator and the particle-particle ladder in the strong-coupling limit [cf. also Eq. (2.12)]. Owing to this difference, $u_2(0)$ given by Eq. (2.30) (and not $\tilde{u}_2(0)$ given by Eq. (2.29)) has to be identified with the boson-boson interaction at zero four-momenta. We shall return to the difference between \tilde{u}_2 and u_2 in subsection IIIB.²⁹

Recalling further that the scattering length a_B^{Born} within the Born approximation, obtained for a pair of true bosons (each of mass $2m$) mutually interacting via a two-body potential with Fourier transform $u_2(0)$ at zero wave vector, is given by $a_B^{\text{Born}} = 2m u_2(0) / (4\pi)$, Eq. (2.30) yields the following relation between the bosonic and fermionic scattering lengths:

$$a_B^{\text{Born}} = 2 a_F. \quad (2.31)$$

The result (2.31) was also obtained in Ref. 9 within the fermionic self-consistent T-matrix approximation (which corresponds to the bosonic Hartree-Fock approximation of Fig. 5 in the strong-coupling limit - see the next subsection), where it was regarded to be the value of the scattering length a_B for a “dilute” system of composite bosons. We will show in Section IV that the result (2.31) actually differs from a_B , when *all* diagrams associated with a “dilute” system of composite bosons are taken into account.

Beside the four-point vertex (2.28), the composite nature of the bosons produces (an infinite set of) additional vertices. Let us consider, in particular, the six-point vertex defined by keeping the terms with $l = 3$ in Eq. (2.21). We obtain:

$$S_{\text{eff}}^{(6)} = \frac{1}{6} \text{tr} X^6 = \frac{1}{6(\beta\mathcal{V})^2} \sum_{q_1 \dots q_6} \times \tilde{u}_3(q_1 \dots q_6) b^*(q_1) b^*(q_2) b^*(q_3) b(q_4) b(q_5) b(q_6) \quad (2.32)$$

where the (six-point) *effective three-boson interaction* is given by [cf. Fig. 3]

$$\begin{aligned} \tilde{u}_3(q_1 \dots q_6) &= \delta_{q_1+q_2+q_3, q_4+q_5+q_6} \left(\frac{\mathcal{V}}{\beta} \right)^3 \frac{2}{\beta\mathcal{V}} \sum_k \\ &\times \frac{(-1)}{\epsilon(-k)\epsilon(k+q_2)\epsilon(-k-q_2+q_5)} \\ &\times \frac{1}{\epsilon(k+q_2+q_3-q_5)\epsilon(-k+q_1-q_4)\epsilon(k+q_4)}. \end{aligned} \quad (2.33)$$

In the strong-coupling limit, whereby $|\mu|$ is the relevant energy scale in the problem, from dimensional considerations we get $\tilde{u}_2(\beta/\mathcal{V})^2 \sim |\mu|^{-3/2}$ and $\tilde{u}_3(\beta/\mathcal{V})^3 \sim |\mu|^{-7/2}$

(in three dimensions). For this reason, the contribution of the tree-boson vertex (2.33) is suppressed with respect to the contribution of the two-boson vertex (2.28). To be more precise, one should compare the values of similar diagrams constructed with the four- and six-point vertices, respectively (like, for instance, the ones depicted in Fig. 5 and Fig. 6). The value of the diagram of Fig. 6 is smaller than the value of the diagram of Fig. 5 by the quantity

$$\frac{|\mu|^{-7/2} \epsilon_F^3 |\mu|}{|\mu|^{-3/2} \epsilon_F^{3/2} |\mu|^{1/2}} \sim (k_F a_F)^3. \quad (2.34)$$

Here, the factors containing the Fermi energy $\epsilon_F [= k_F^2 / (2m) = (3\pi^2 \rho)^{2/3} / (2m)]$ originate from the bosonic cycles (cf. Section III), while the factors $|\mu|$ and $|\mu|^{1/2}$ originate from the residue in Eq. (2.12). The diagram of Fig. 6 can thus be neglected in comparison to the diagram of Fig. 5, since $k_F a_F \ll 1$ in the strong-coupling limit.

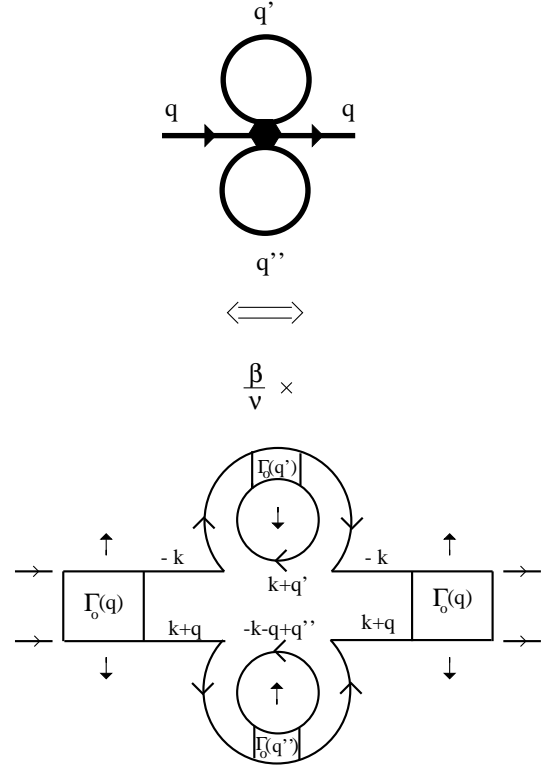


FIG. 6. Graphical correspondence between the composite-boson propagator and the two-fermion Green's function in the particle-particle channel, to first order in the *six-point* interaction vertex. This vertex can be identified from Fig. 3 by setting $q_2 = q_6 = q$, $q_1 = q_4 = q'$, and $q_3 = q_5 = q''$ therein.

The above argument can be made more general, by showing that *all interaction vertices can be neglected in comparison with the four-point vertex in the strong-coupling limit*.³⁰ In this limit, one can thus construct all diagrams representing the two-particle Green's function in the particle-particle channel in terms of the “bare”

ladder and of the four-point interaction vertex only. This is precisely what one would expect on physical grounds, since the interactions involving more than two bodies become progressively less effective as the composite bosons overlap less when approaching the strong-coupling limit. However, it is also clear from the above considerations that in the *extreme* strong-coupling limit (whereby $a_F \rightarrow 0$) the four-point vertex can be neglected, too, and the composite bosons become *effectively free*.¹⁴

In the next subsection we will show how the (self-consistent) fermionic T-matrix approximation can be examined in terms of the four, six, \dots , -vertex functions in the strong-coupling limit.

C. Fermionic T-matrix approximation in the strong-coupling limit

The T-matrix approximation for a “dilute” Fermi gas represents one of the few cases in the many-body theory where the choice of the self-energy diagrams can be controlled by an external small parameter.³¹ In the original version by Galitskii,⁶ the T-matrix approximation was conceived for a *repulsive* fermionic interaction of finite range (thus excluding bound states) and with the scattering length a_F always positive (albeit small). The fermionic self-energy diagram associated with this approximation is depicted at the left in Fig. 7a, and is obtained by closing the particle-particle ladder with a single-particle Green’s function in the only possible way. [The diagram at the right in Fig. 7a was included by Galitskii original treatment,⁶ but vanishes for our choice of the attractive potential since it contains forbidden interactions between parallel spins. By the same token, no spin summation needs to be considered for the fermionic loop at the left in Fig. 7a.] In Fig. 7a all single-particle lines are regarded to be *self-consistent*, and thus contain self-energy insertions of the same kind of the ones depicted in the figure.³² In this way, the self-consistent fermionic T-matrix is “conserving” in the Baym-Kadanoff sense.^{22,23} Recalling that (with our regularization of the potential) the particle-particle ladder depends only on the sum of the incoming (outgoing) four-momenta, the self-energy of Fig. 7a reads

$$\Sigma_F(k) = -\frac{1}{\beta\mathcal{V}} \sum_{k'} \Gamma_s(k+k') \mathcal{G}(k') \quad (2.35)$$

where Γ_s is obtained from Γ_o by replacing everywhere the “bare” \mathcal{G}_o with the self-consistent \mathcal{G} .

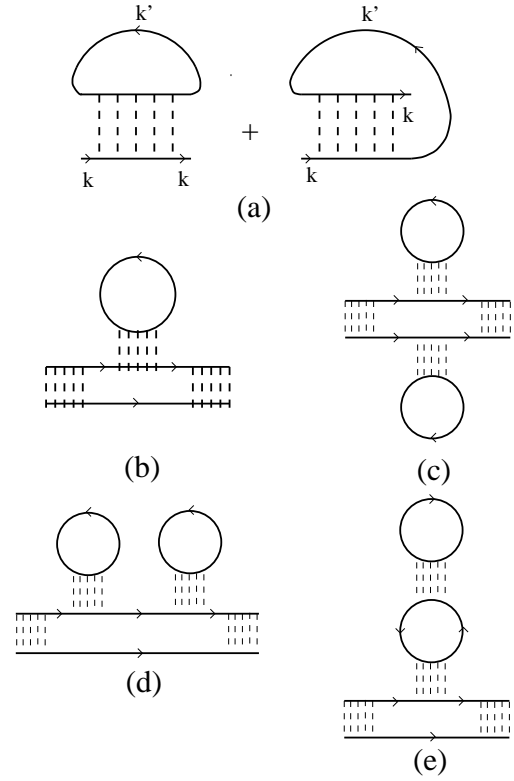


FIG. 7. (a) Self-energy diagrams corresponding to the self-consistent fermionic T-matrix approximation (full lines here represent self-consistent fermionic single-particle Green’s functions and spin labels have been suppressed); Self-energy corrections entering the particle-particle ladder, obtained by contracting the (b) four-point vertex and (c-e) six-point vertex (full lines now represent the “bare” fermionic single-particle Green’s functions).

In the approximation of the lowest order, self-energy insertions are neglected and the “full” single-particle lines of Fig. 7a are replaced by “bare” ones. The particle-particle ladder Γ_s of Eq. (2.35) thus reduces to Γ_o of Fig. 2a, which (apart from a sign) is approximately given by Eq. (2.10) in the weak-coupling limit (irrespective of the sign of a_F). We thus obtain to this order:

$$\Sigma_F^{(o)}(k) = \frac{4\pi a_F}{m} \frac{\rho}{2} = \epsilon_F \left(\frac{4}{3\pi} k_F a_F + \mathcal{O}((k_F a_F)^2) \right) \quad (2.36)$$

where the density factor $\rho [= k_F^3/(3\pi^2)]$ is supplied by the closed fermionic loop. Considering self-energy insertions on top of the result (2.36) modifies Σ_F/ϵ_F only to $\mathcal{O}((k_F a_F)^2)$.

For the *attractive* fermionic interaction of interest, the scattering length a_F changes from being negative when the two-body problem fails to support a bound state, to being positive when the bound state is eventually supported by increasing the interaction strength. As already discussed in subsection IIA, the sign change of a_F has dramatic effects on the “bare” particle-particle

ladder Γ_o , that changes from the behavior (2.10) in the weak-coupling limit to developing a polar structure in the strong-coupling limit (cf. Eq. (2.12)). In the latter limit, the self-energy $\Sigma_F^{(o)}$ acquires the density factor from the particle-particle ladder and not from the closed fermionic loop. This can be explicitly seen by transforming the Matsubara frequency sum in the expression for $\Sigma_F^{(o)}$ into a contour integration in the complex frequency plane as follows:

$$\Sigma_F^{(o)}(k) = -\frac{1}{\beta\mathcal{V}} \sum_{k'} \Gamma_o(k+k') \mathcal{G}^o(k') = -\int \frac{d\mathbf{k}'}{(2\pi)^3} \times \oint_C \frac{dz}{2\pi i} \Gamma_o(\mathbf{k}+\mathbf{k}', z) \mathcal{G}^o(\mathbf{k}', z - i\omega_n) \frac{1}{e^{\beta z} - 1} \quad (2.37)$$

where C is a contour encircling the imaginary axis in the positive sense. In the strong-coupling limit, $\mathcal{G}^o(\mathbf{k}', z - i\omega_n)$ has a pole for $\text{Re}(z) \geq |\mu|$, so that the contribution of this pole to the integral in Eq. (2.37) is strongly reduced by the Bose factor $\exp\{-\beta|\mu|\}$. The dominant contribution to the integral in Eq. (2.37) thus comes from the pole of $\Gamma_o(\mathbf{k}+\mathbf{k}', z)$, yielding

$$\begin{aligned} \Sigma_F^{(o)}(k) &\cong \frac{8\pi}{m^2 a_F} \int \frac{d\mathbf{k}'}{(2\pi)^3} \frac{1}{i\omega_n + \xi(\mathbf{k}') - \frac{(\mathbf{k}+\mathbf{k}')^2}{4m}} \\ &\times \frac{1}{e^{\beta(\mathbf{k}+\mathbf{k}')^2/(4m)} - 1} \\ &\approx \frac{8\pi}{m^2 a_F} \frac{1}{i\omega_n + \xi(\mathbf{k})} \frac{\rho}{2}. \end{aligned} \quad (2.38)$$

It is interesting to note that the expression (2.38) for the self-energy leads to a *double-fraction structure* in the single-particle fermionic Green's function, since

$$\mathcal{G}(\mathbf{k}, \omega_n) = \frac{1}{i\omega_n - \xi(\mathbf{k}) - \frac{B}{i\omega_n + \xi(\mathbf{k})}} \quad (2.39)$$

with $B = 4\pi\rho/(m^2 a_F)$. It is then clear that the expression (2.39) has the form of the BCS Green's function, namely,

$$\mathcal{G}(\mathbf{k}, \omega_n) = \frac{u^2(\mathbf{k})}{i\omega_n - E(\mathbf{k})} + \frac{v^2(\mathbf{k})}{i\omega_n + E(\mathbf{k})}, \quad (2.40)$$

where

$$E(\mathbf{k}) = \sqrt{\xi^2(\mathbf{k}) + B} \quad (2.41)$$

has a gap given approximately by $|\mu| + B/(2|\mu|)$ and where

$$v^2(\mathbf{k}) = 1 - u^2(\mathbf{k}) \cong \frac{4}{3\pi} \frac{(k_F a_F)^3}{[1 + (|\mathbf{k}| a_F)^2]^2}. \quad (2.42)$$

Besides the main peak at $E(\mathbf{k})$ (with weight $u^2(\mathbf{k})$), the spectral function associated with the Green's function (2.40) has also a secondary peak at $-E(\mathbf{k})$ (with

weight $v^2(\mathbf{k})$). This secondary peak is relevant to photoemission experiments and can be interpreted as a “shadow-band” structure, associated with a real gap in the single-particle spectrum; this gap, in turn, might be regarded as anticipating the pseudo-gap actually observed in ARPES experiments above the superconducting transition temperature.^{2,3} It is also for this promising feature that several authors have considered the fermionic T-matrix approximation as representing the “dilute-approach approximation” for the BCS-BE crossover problem.⁸⁻¹³

Self-energy insertions associated with the self-consistency of the fermionic single-particle Green's function modify both Γ_o and \mathcal{G}^o in Eq. (2.37). As far as the self-energy insertions on Γ_o are concerned, they can be interpreted in terms of the four, six, \dots , -point interaction vertices discussed in the previous subsections. Typical examples are shown in Figs. 7b-e, where the “bare” single-particle lines associated with the vertices are marked by arrows. Note, in particular, that the diagram of Fig. 7b corresponds to a contraction of the four-point vertex, while the diagrams of Figs. 7c-e correspond to all possible contractions of the six-point vertex. Additional diagrams not shown in the figure would then contain interaction vertices of higher order. Note also that the diagrams of Figs. 7b-c have been already considered in Fig. 5 and in Fig. 6, respectively. From the results of the previous subsection we then conclude that only the diagram of Fig. 7b needs to be retained in the strong-coupling limit, the other diagrams being suppressed with respect to it at least by a factor $(k_F a_F)^3$ (cf. Eq. (2.34)). The diagram of Fig. 7b corresponds to the Hartree-Fock approximation for the self-energy of composite bosons.¹⁹ Note finally that self-energy insertions on \mathcal{G}^o in Eq. (2.37) could be interpreted similarly, in an open-ended way.

The above argument leads us to the conclusion that the fermionic T-matrix approximation reproduces the Hartree-Fock approximation to the self-energy of composite bosons in the strong-coupling limit. This self-energy modifies the pole of Γ_o in Eq. (2.37) and affects eventually the (pseudo) gap structure in the fermionic self-energy. There exist, however, *additional* contributions to the self-energy of composite bosons which are of the *same order* (in the small parameter $k_F a_F$) of the Hartree-Fock approximation just discussed. These contributions are not included in the fermionic T-matrix approximation and must be considered separately, as shown in the next Section.

III. T-MATRIX APPROXIMATION FOR COMPOSITE BOSONS

In this Section we shall set up an approximation for the fermionic self-energy, which describes the “low-density” regime *both* in the weak-coupling (fermionic) and in the strong-coupling (bosonic) limits on equal footing. To

this end, we rely on the results of the previous Section and consider first the construction of the two-fermion Green's function in the bosonic limit, in terms of the “bare” particle-particle ladder and of the effective two-boson interaction. Before examining this procedure in detail, however, it is instructive to briefly recall some well-known results concerning the self-energy for a “dilute” system of true (point-like) bosons,^{7,20,21} and in particular the method for selecting the relevant self-energy diagrams for this system. In this way, we will learn how to generalize this method to the case of a “dilute” system of composite bosons, for which the effective two-boson interaction depends on frequency as well as on wave vector.

We will eventually extrapolate the approximation thus obtained from the bosonic to the (fermionic) weak-coupling limit through the crossover region. In the latter region (where the parameter $k_F a_F$ exceeds unity), however, the “low-density” approximation has to be regarded merely as a scheme which interpolates between the two controlled limits.

A. Low-density approximation for true (point-like) bosons

The standard argument to select the diagrams giving the leading contribution to the self-energy for a “low-density” Bose gas proceeds as follows.^{7,20,21} Let $u(\mathbf{q}_1, \mathbf{q}_2, \mathbf{q}_3, \mathbf{q}_4)$ be the (symmetrized) bosonic interaction potential, assumed to be vanishing for $|\mathbf{q}_i| \gtrsim r_o^{-1}$ ($i = 1, \dots, 4$), where r_o is the range of the potential. We shall also consider temperatures not too higher than the BE critical temperature, so that we shall assume $T \sim \rho^{2/3}$. Under these conditions, it turns out that *every cycle in a diagram contributes a factor $T^{3/2} \sim \rho^{33}$*

To show this, we consider the generic self-energy diagram of Fig. 8a, containing one closed path constructed with “bare” bosonic propagators. We perform explicitly the sum over the four-momentum \mathbf{q} running along the cycle. Let $\xi_B(\mathbf{q}) = \mathbf{q}^2/(2m_B) - \mu_B$, where m_B is the bosonic mass and μ_B the bosonic chemical potential, respectively. To the diagram of Fig. 8a we then associate the expression

$$\mathcal{L}(\mathbf{q}_{ext}) = \sum_{P, Q} \mathcal{F}(P, Q) \sum_{\mathbf{q}} U(\mathbf{q}; \mathbf{Q}) \frac{1}{i\Omega_\nu - \xi_B(\mathbf{q})} \quad (3.1)$$

$$\times \frac{1}{i(\Omega_\nu + \Omega_{\nu_1}) - \xi_B(\mathbf{q} + \mathbf{q}_1)} \cdots \frac{1}{i(\Omega_\nu + \Omega_{\nu_r}) - \xi_B(\mathbf{q} + \mathbf{q}_r)}$$

where $U(\mathbf{q}; \mathbf{Q})$ stands for the product of all interaction potentials attached to the cycle (with all wave vectors other than \mathbf{q} indicated collectively by \mathbf{Q}) and $\mathcal{F}(P, Q)$ for the expression of the rest of the diagram (appropriate factors $(\beta\mathcal{V})^{-1}$ are understood to be associated with the four-momentum sums).

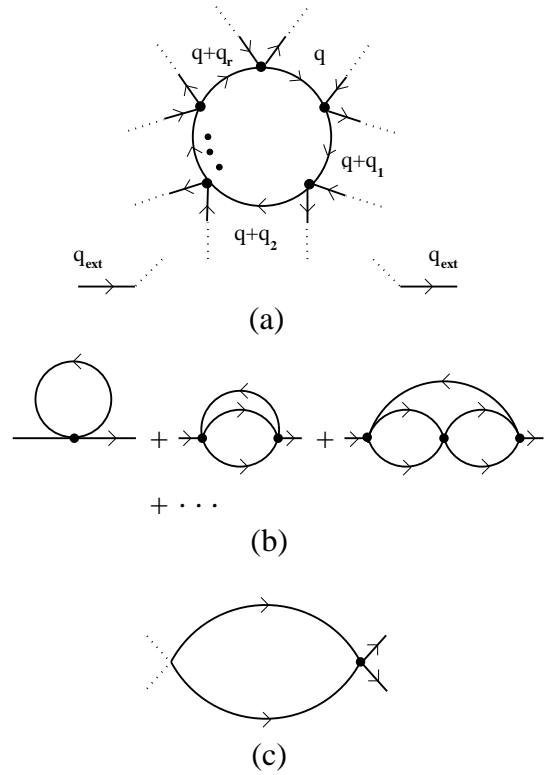


FIG. 8. (a) Generic self-energy diagram for a system of *true* bosons, containing one cycle (full lines and full circles here stand for the “bare” bosonic propagators and the (symmetrized) interaction potential, respectively, while dotted lines represent connections to the rest of the diagram); (b) T-matrix approximation to the self-energy of true bosons; (c) Elementary rung for the bosonic T-matrix.

The sum over the Matsubara frequency Ω_ν can be readily performed in Eq. (3.1), since the interaction potential for point-like bosons is frequency independent. For this sum we obtain the result:

$$-\frac{1}{e^{\beta\xi_B(\mathbf{q})} - 1} \frac{1}{\xi_B(\mathbf{q}) + i\Omega_{\nu_1} - \xi_B(\mathbf{q} + \mathbf{q}_1)} \cdots$$

$$\times \frac{1}{\xi_B(\mathbf{q}) + i\Omega_{\nu_r} - \xi_B(\mathbf{q} + \mathbf{q}_r)}$$

$$-\frac{1}{e^{\beta\xi_B(\mathbf{q} + \mathbf{q}_1)} - 1} \frac{1}{\xi_B(\mathbf{q} + \mathbf{q}_1) - i\Omega_{\nu_1} - \xi_B(\mathbf{q})} \cdots$$

$$\times \frac{1}{\xi_B(\mathbf{q} + \mathbf{q}_1) + i(\Omega_{\nu_r} - \Omega_{\nu_1}) - \xi_B(\mathbf{q} + \mathbf{q}_r)} - \cdots \quad (3.2)$$

When integrating further over the wave vector \mathbf{q} in Eq. (3.1) (and provided μ_B is negative), each Bose factor in Eq. (3.2) introduces a *cutoff* proportional to $T^{1/2} \sim \rho^{1/3}$ about $\mathbf{q} + \mathbf{q}_j \approx 0$ (with $\mathbf{q}_j = 0, \mathbf{q}_1, \dots, \mathbf{q}_r$). This cutoff is much smaller than the range r_o^{-1} of the bosonic interaction potential, owing to the “low-density” condition $\rho^{1/3} r_o \ll 1$. We can then approximate $\mathbf{q} \approx 0$ everywhere in the integrand associated with the first term of Eq. (3.2), $\mathbf{q} + \mathbf{q}_1 \approx 0$ in the integrand associated with the second term of Eq. (3.2), and so on, *except* for the Bose

factors that retain the wave vector dependence indicated in Eq. (3.2). We thus obtain the following approximate result for the sum over q in the expression (3.1):

$$\begin{aligned}
& - \frac{1}{i\Omega_{\nu_1} - \frac{\mathbf{q}_1^2}{2m_B}} \cdots \frac{U(0; \mathbf{Q})}{i\Omega_{\nu_r} - \frac{\mathbf{q}_r^2}{2m_B}} \int \frac{d\mathbf{q}}{(2\pi)^3} \frac{1}{e^{\beta\xi_B(\mathbf{q})} - 1} \\
& - \frac{1}{-i\Omega_{\nu_1} - \frac{\mathbf{q}_1^2}{2m_B}} \cdots \frac{U(-\mathbf{q}_1; \mathbf{Q})}{i(\Omega_{\nu_r} - \Omega_{\nu_1}) - \frac{(\mathbf{q}_r - \mathbf{q}_1)^2}{2m_B}} \\
& \times \int \frac{d\mathbf{q}}{(2\pi)^3} \frac{1}{e^{\beta\xi_B(\mathbf{q} + \mathbf{q}_1)} - 1} - \cdots
\end{aligned} \quad (3.3)$$

where each integral equals the bosonic density $\rho_B = \rho/2$. For generic values of the wave vectors $\mathbf{q}_1, \dots, \mathbf{q}_r$ and of the frequencies $\Omega_{\nu_1}, \dots, \Omega_{\nu_r}$ entering Eq. (3.1), each term in Eq. (3.3) is thus proportional to the density. The presence of one cycle in Eq. (3.1) makes, in turn, the whole expression proportional to ρ .

It then follows that, for a “low-density” Bose system, the leading self-energy diagrams contain the *minimum number* of cycles, like the diagrams shown in Fig. 8b, which constitutes the so-called bosonic T-matrix approximation.^{7,20,21} It is interesting to contrast the behaviour of the cycle (whereby the Bose factor introduces a cutoff proportional to $T^{1/2} \sim \rho^{1/3}$) with the behaviour of an elementary rung (drawn in Fig. 8c) in the diagrammatic representation of the bosonic T-matrix, with one potential vertex and two bosonic propagators running in the *same* direction. In this case, the cutoff originates from the potential and *not* from the Bose factor. Let us, in fact, assume, for simplicity, that the bosonic interaction potential is (approximately) constant ($\sim u(0)$) up to the cutoff r_o^{-1} . It can then be readily shown that, at low enough temperature, the dominant contribution to the diagram of Fig. 8c is given by $u(0)r_o^{-1}$, in analogy with the result (2.5) for fermions. No density factor thus arises in this case.

To generalize the above results to a “dilute” system of *composite* bosons, it is essential to take into account the *frequency dependence* of the effective two-boson interaction (2.28), which makes the calculation of the analogue of the expression (3.1) somewhat more involved. We will, however, show in the next subsection that this quantity remains proportional to ρ .

B. Low-density approximation for composite bosons

The generic self-energy diagram containing one cycle and associated with the propagator $\langle b^*(q)b(q) \rangle_{S_{\text{eff}}}$ for composite bosons is shown in Fig. 9a. Here, thick lines and squares represent the “bare” propagator $\langle b^*(q)b(q) \rangle_{S_{\text{eff}}^{(2)}}$ of Eq. (2.26) for composite bosons and the effective two-boson interaction given by Eq. (2.28), respectively, according to the conventions of Fig. 4. [Recall from subsection IIB that only the two-boson interaction needs to be taken into account in the strong-coupling limit.]

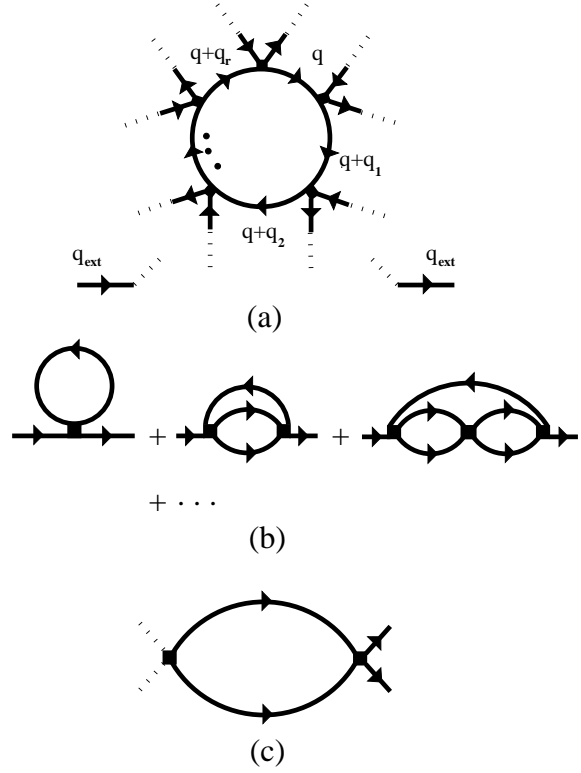


FIG. 9. (a) Generic self-energy diagram for a system of *composite* bosons, containing one cycle (thick lines and full squares stand for the “bare” propagators for composite bosons and the effective two-boson interaction, respectively, according to the conventions of Fig. 4, while dotted lines represent connections to the rest of the diagram); (b) T-matrix approximation to the self-energy of composite bosons; (c) Elementary rung for the T-matrix of composite bosons.

The expression of the “bare” propagator $\langle b^*(q)b(q) \rangle_{S_{\text{eff}}^{(2)}}$ is obtained by inserting in Eqs. (2.26) and (2.7) the expression (2.11) for R_{pp} , that holds specifically in the strong-coupling limit (whereby $\beta\mu \rightarrow -\infty$). Writing $\sqrt{E_\alpha} \text{sgn}(\text{Im} E_\alpha) = i\sqrt{-E_\alpha}$ and recalling the definition (2.9) for E_α , we obtain:

$$\begin{aligned}
\langle b^*(q)b(q) \rangle_{S_{\text{eff}}^{(2)}} &= \frac{\beta}{\mathcal{V}} \frac{-1}{\frac{m}{4\pi a_F} - \frac{m^{3/2}}{4\pi} \sqrt{-i\Omega_\nu + \frac{\mathbf{q}^2}{4m} - 2\mu}} \\
&= \frac{D(q)}{i\Omega_\nu - \left(\frac{\mathbf{q}^2}{4m} - \mu_B \right)}, \quad (3.4)
\end{aligned}$$

where we have used the definition $\mu_B = 2\mu + \epsilon_o$ for the bosonic chemical potential and introduced the notation³⁴

$$D(q) = -\frac{\beta}{\mathcal{V}} \frac{4\pi}{m^2 a_F} \left(1 + \sqrt{1 + \frac{-i\Omega_\nu + \frac{\mathbf{q}^2}{4m} - \mu_B}{\epsilon_o}} \right). \quad (3.5)$$

Replacing further $i\Omega_\nu$ by the complex frequency z , we note that, near the position $z = \mathbf{q}^2/(4m) - \mu_B$ of the

pole in Eq. (3.4), $D(q)$ of Eq. (3.5) reduces to $(-\beta/\mathcal{V})$ times the constant value $8\pi/(m^2 a_F)$ entering Eq. (2.12) and thus plays the role of a residue. Away from this pole, $D(q)$ has a cut along the positive real axis for $\text{Re}(z) \geq -2\mu$.

To retain the structure of Eq. (3.1) as close as possible (with $m_B = 2m$ in the “bare” bosonic propagators), it is convenient to transfer the factors $D(q)$ from the “bare” propagators $\langle b^*(q)b(q) \rangle_{S_{\text{eff}}^{(2)}}$ to the effective two-boson interactions, which these propagators are joined to. Specifically, every propagator $\langle b^*(q)b(q) \rangle_{S_{\text{eff}}^{(2)}}$ associated with an “internal” line of a diagram transfers a factor $\sqrt{D(q)}$ to each of the two interaction vertices it is joined to, while each propagator associated with one of the two “external” lines transfers one factor $\sqrt{D(q)}$ to the single interaction it is joined to and assigns the remaining factor $\sqrt{D(q)}$ as a proportionality factor to the “full” propagator, which the diagram is meant to represent. In this way, the “full” propagator acquires the same overall factor $D(q)$ of the “bare” propagator (3.4) and the effective two-boson interaction of Eq. (2.28) is multiplied by $\sqrt{D(q_1)}\sqrt{D(q_2)}\sqrt{D(q_3)}\sqrt{D(q_4)}$. We are then led to *rescaling* the effective two-boson interaction as follows

$$2u_2(q_1 \dots q_4) \quad (3.6)$$

$$\equiv \tilde{u}_2(q_1 \dots q_4) \sqrt{D(q_1)} \sqrt{D(q_2)} \sqrt{D(q_3)} \sqrt{D(q_4)}$$

with $\tilde{u}_2(q_1 \dots q_4)$ given by Eq. (2.28). [Note that the above definition accounts, in particular, for the difference between $\tilde{u}_2(0)$ and $u_2(0)$ in Eq. (2.29).]

To the generic self-energy diagram of Fig. 9a, containing one cycle of “bare” propagators for composite bosons, we thus associate an expression similar to (3.1), namely,

$$\mathcal{L}(\mathbf{q}_{\text{ext}}) = \sum_{P,Q} \mathcal{F}(P,Q) \sum_q U(q;Q) \frac{1}{i\Omega_\nu - \xi_B(\mathbf{q})} \quad (3.7)$$

$$\times \frac{1}{i(\Omega_\nu + \Omega_{\nu_1}) - \xi_B(\mathbf{q} + \mathbf{q}_1)} \dots \frac{1}{i(\Omega_\nu + \Omega_{\nu_r}) - \xi_B(\mathbf{q} + \mathbf{q}_r)}$$

where $U(q;Q)$ now stands for the product of all rescaled effective two-boson interactions $2u_2$ attached to the cycle. Although the sum over the Matsubara frequency Ω_ν in Eq. (3.7) cannot be performed explicitly as we have done in Eq. (3.1), it can be conveniently transformed into a contour integration as in Eq. (2.37). We thus obtain for this frequency sum:

$$\oint_C \frac{dz}{2\pi i} \frac{1}{z - \xi_B(\mathbf{q})} \frac{1}{z + i\Omega_{\nu_1} - \xi_B(\mathbf{q} + \mathbf{q}_1)} \dots$$

$$\times \frac{1}{z + i\Omega_{\nu_r} - \xi_B(\mathbf{q} + \mathbf{q}_r)} \frac{U(\mathbf{q}, z; Q)}{e^{\beta z} - 1}. \quad (3.8)$$

To proceed further, we need to spell out the analytic properties of $U(\mathbf{q}, z; Q)$. From Fig. 9a one realizes that *each* factor \tilde{u}_2 entering the expression for U in Eq. (3.7) has the following structure [cf. Eq. (2.28)]:

$$\tilde{u}_2(q + q_j, q_a, q_b, q + q_{j-1}) = \delta_{q_j + q_a, q_{j-1} + q_b} \left(\frac{\mathcal{V}}{\beta} \right)^2 \frac{2}{\beta \mathcal{V}}$$

$$\times \sum_k \frac{1}{\epsilon(-k)\epsilon(k + q_a)\epsilon(-k + q_j - q_{j-1})\epsilon(k + q + q_{j-1})} \quad (3.9)$$

where q_a and q_b belong to the set Q of Eq. (3.7). In other words, the cycle variable q in Eq. (3.9) appears *only* in the last factor $\epsilon(k + q + q_{j-1})^{-1}$. Viewed as a function of the complex variable z of Eq. (3.8), each factor \tilde{u}_2 has thus a *cut* along the positive real axis for $\text{Re}(z) \geq -\mu$. This property, in turn, remains true for the rescaled effective two-boson potential u_2 of Eq. (3.6), since we have already determined that the factor $D(q)$ has itself a cut along the positive real axis for $\text{Re}(z) \geq -2\mu$.

It is thus clear that the contribution of the singularities of $U(\mathbf{q}, z; Q)$ to the integral of Eq. (3.8) is strongly suppressed by the presence of the Bose factor $(\exp\{\beta z\} - 1)^{-1}$ therein, since $\beta|\mu| \gg 1$ in the strong-coupling limit. In this limit, the contribution of these singularities can then be neglected, with the result that the value of the expression (3.7) is proportional to the bosonic density ρ_B , by the very argument discussed in the previous subsection for point-like bosons.

We conclude that, for a system of composite bosons in the “low-density” limit, the leading diagrams contain just *one cycle*, like the ones shown in Fig. 9b. In analogy with the corresponding diagrams of Fig. 8b for point-like bosons, we shall refer to these diagrams as the T-matrix approximation for composite bosons.

That in the strong-coupling limit all diagrams of Fig. 9b are of the *same order* (in the original fermionic parameter $k_F a_F$ - cf. Ref. 14) can be further verified as follows. Consider the elementary rung (drawn in Fig. 9c) in the diagrammatic representation of the T-matrix for composite bosons. We know that the interaction vertex u_2 scales as $|\mu|^{-3/2} \times a_F^{-2}$ in the strong-coupling limit, where the factor $|\mu|^{-3/2}$ stems from the behaviour of \tilde{u}_2 (cf. the comment after Eq. (2.33)) and the factor a_F^{-2} from the presence of two powers of D in the definition (3.6) of the rescaled interaction vertex u_2 (cf. also Eq. (3.5)). By the argument made for point-like bosons at the end of the previous subsection, the cut-off on the four-momentum of the rung is provided by the interaction vertex since the two “bare” propagators for composite bosons run in the same direction. This four-momentum sum is then proportional to the cut-off of the interaction vertex, which we know from Ref. 16 to be given by a_F^{-1} . Putting all factors together and recalling that $|\mu|^{-1/2} \propto a_F$ in the strong-coupling limit, we obtain that the rung of Fig. 9c scales like $|\mu|^{-3/2} \times a_F^{-2} \times a_F^{-1} \sim \text{constant}$. This result implies that the order of the diagram in the parameter $k_F a_F$ is not altered by the insertion of an *arbitrary number* of these rungs.

The diagrams of Fig. 9 have been drawn in terms of propagators and interaction vertices for composite bosons. When extrapolating these diagrams from the

bosonic to the fermionic (weak-coupling) limit through the crossover region, however, it will be useful to draw them also in the alternative representation in terms of the constituent fermions, via the correspondence rules of Fig. 4. In Appendix B we will examine in detail which fermionic diagrams are associated with the T-matrix approximation for composite bosons. In this way, we shall relate the value of the symmetry factors of the bosonic diagrammatic structure with the number of independent diagrams in the corresponding fermionic diagrammatic structure. We shall also show that in the weak-coupling limit, where the composite-boson propagator becomes a constant to leading-order in $k_F a_F$ (cf. Eq. (2.10)), our generalized T-matrix approximation reduces correctly to the Galitskii approximation for the self-energy of a “low-density” Fermi gas.

C. Coupled equations defining the generalized T-matrix approximation for the BE-BCS crossover

Once the self-energy diagrams for composite bosons in the “low-density” limit have been selected according to the above prescriptions, there remains to determine the analytic expression of these diagrams. To this end, it is convenient to stick with the bosonic representation and write down the expression for the bosonic propagator $< b^*(q)b(q) >_{S_{\text{eff}}}$ with the self-energy insertions of Fig. 9b, making use of the standard bosonic diagrammatic rules.^{20,21} Recalling the general relation (A7) of Appendix A for the “full” bosonic propagator (as well as its counterpart (2.26) for the “bare” bosonic propagator), we obtain:

$$\begin{aligned} \frac{\beta}{\mathcal{V}}\Gamma(q) &= \frac{\beta}{\mathcal{V}} \left\{ \Gamma_o(q) - \Gamma_o(q)^2 \frac{1}{\beta\mathcal{V}} \sum_{q'} \Gamma_o(q') \right. \\ &\times \left[\mathcal{S}_1 2\bar{u}_2(q', q, q, q') - \frac{\mathcal{S}_2}{\beta\mathcal{V}} \sum_{q_1} 2\bar{u}_2(q', q, q_1, q + q' - q_1) \right. \\ &\times \Gamma_o(q_1) \Gamma_o(q + q' - q_1) 2\bar{u}_2(q + q' - q_1, q_1, q, q') \\ &+ \frac{\mathcal{S}_3}{(\beta\mathcal{V})^2} \sum_{q_1, q_2} 2\bar{u}_2(q', q, q_2, q + q' - q_2) \Gamma_o(q_2) \Gamma_o(q + q' - q_2) \\ &\times 2\bar{u}_2(q + q' - q_2, q_2, q_1, q + q' - q_1) \Gamma_o(q_1) \Gamma_o(q + q' - q_1) \\ &\times 2\bar{u}_2(q + q' - q_1, q_1, q, q') - \dots \left. \right] + \dots \left. \right\}. \quad (3.10) \end{aligned}$$

In this expression, $\mathcal{S}_L = 2^{1-L} (L = 1, 2, \dots)$ is the *symmetry factor* associated with the bosonic self-energy diagram of Fig. 9b containing L bosonic interaction vertices [cf. Appendix B], \bar{u}_2 is proportional to the effective two-boson interaction of Eq. (2.28)

$$\begin{aligned} \bar{u}_2(q_1 \dots q_4) &= \frac{1}{\beta\mathcal{V}} \sum_k \frac{1}{\epsilon(-k)\epsilon(k+q_2)\epsilon(-k+q_1-q_4)\epsilon(k+q_4)}, \quad (3.11) \end{aligned}$$

and Γ_o is the “bare” particle-particle ladder of Fig. 2a, whose complete expression

$$\begin{aligned} \Gamma_o(q) &= - \left\{ \frac{m}{4\pi a_F} + \int \frac{d\mathbf{k}}{(2\pi)^3} \right. \\ &\times \left[\frac{\tanh(\beta\xi(\mathbf{k})/2) + \tanh(\beta\xi(\mathbf{k}-\mathbf{q})/2)}{2(\xi(\mathbf{k}) + \xi(\mathbf{k}-\mathbf{q}) - i\Omega_\nu)} - \frac{m}{\mathbf{k}^2} \right] \left. \right\}^{-1} \quad (3.12) \end{aligned}$$

holds irrespective of the value of a_F and reduces in particular to the form (3.4) in the strong-coupling limit $\beta\mu \rightarrow -\infty$.

Note that the factor 2, which entered the definition (2.28) for \bar{u}_2 but has been removed from the definition (3.11) for \bar{u}_2 , multiplies now each \bar{u}_2 in Eq. (3.10) explicitly. These factors of 2 combine with the symmetry factors \mathcal{S}_L in Eq. (3.10), resulting in an overall factor of 2 multiplying the whole expression within brackets therein. This expression corresponds then to the following integral equation

$$\begin{aligned} \bar{t}_B(q_1, q_2, q_3, q_4) &= \bar{u}_2(q_1, q_2, q_3, q_4) \\ &- \frac{1}{\beta\mathcal{V}} \sum_{q_5} \bar{u}_2(q_1, q_2, q_5, q_1 + q_2 - q_5) \Gamma_o(q_5) \Gamma_o(q_1 + q_2 - q_5) \\ &\times \bar{t}_B(q_1 + q_2 - q_5, q_5, q_3, q_4) \quad (3.13) \end{aligned}$$

with $q_1 + q_2 = q_3 + q_4$, provided we set $q_1 = q_4 = q'$ and $q_2 = q_3 = q$. Equation (3.13) identifies the *generalized T-matrix for composite bosons*, in analogy with the ordinary T-matrix for true bosons.^{7,20,21} It is thus clear from Eq. (3.10) that the quantity

$$\Sigma_B^{(t)}(q) = - \frac{2}{\beta\mathcal{V}} \sum_{q'} \Gamma_o(q') \bar{t}_B(q', q, q, q') \quad (3.14)$$

represents the T-matrix approximation to the self-energy for composite bosons, in terms of which Eq. (3.10) acquires the characteristic form of a Dyson’s equation:

$$\begin{aligned} \Gamma(q) &= \Gamma_o(q) + \Gamma_o(q) \Sigma_B^{(t)}(q) \Gamma_o(q) + \dots \\ &= \frac{\Gamma_o(q)}{1 - \Sigma_B^{(t)}(q) \Gamma_o(q)} = \frac{1}{\frac{1}{\Gamma_o(q)} - \Sigma_B^{(t)}(q)}. \quad (3.15) \end{aligned}$$

With the above expression for the particle-particle ladder (which, by construction, correctly describes a system of “low-density” composite bosons in the strong-coupling limit), we can obtain the fermionic self-energy of interest in analogy to Eq. (2.35), by joining the incoming and outgoing arrows of the particle-particle ladder Γ with a single-particle fermionic Green’s function in the only possible way. We then write:

$$\Sigma_F(k) = - \frac{1}{\beta\mathcal{V}} \sum_{k'} \Gamma(k+k') \mathcal{G}^o(k') \quad (3.16)$$

with Γ given by Eq. (3.15) and where \mathcal{G}^o is the “bare” single-particle fermionic Green’s function. The

self-energy (3.16) has in turn to be inserted into the fermionic Dyson's equation, to yield the full single-particle fermionic Green's function \mathcal{G} . Eventual extrapolation from the strong- to the weak-coupling limit through the crossover region requires us to eliminate the chemical potential in favor of the particle density ρ , by evaluating

$$\rho = \frac{2}{\beta\mathcal{V}} \sum_k e^{i\omega_n\eta} \mathcal{G}(k) \quad (3.17)$$

where η is a positive infinitesimal.

Besides the explicit \mathcal{G}^o in Eq. (3.16), also *all* single-particle fermionic Green's functions entering the expression (3.15) for Γ are meant to be “bare” ones, in analogy to the original approach by Galitskii.³² We expect, in fact, that the inclusion of self-consistency in the explicit single-particle fermionic Green's function of Eq. (3.16) should not be essential to represent correctly the fermionic self-energy, either in the strong-coupling limit (where, on physical grounds, it is rather the bosonic propagator that needs to be represented correctly) or in the weak-coupling limit (where self-consistency drops out anyway for a “low-density” Fermi system). [In addition, in the crossover region (where our “low-density” approximation merely interpolates between the two controlled limits) inclusion of self-consistency should not be of primary concern.] By the same token, inclusion of self-consistency in the single-particle fermionic Green's functions entering the expression (3.15) for Γ would yield contributions of higher order in the small parameter $k_F a_F$ with respect to the ones retained (both in the weak- and strong-coupling limits).

The question of self-consistency in the single-particle fermionic Green's function is also connected with the general requirement for an approximation to the fermionic self-energy to be “conserving” in the Baym-Kadanoff sense.^{22,23} According to this requirement, once an approximation has been selected by physical considerations *at the level of* the fermionic two-particle Green's function (in the particle-particle channel), one should in principle construct a functional Φ such that the fermionic self-energy itself is, in turn, obtained by taking the functional derivative of Φ with respect to the self-consistent \mathcal{G} . It is obvious that this procedure yields several *additional* self-energy terms, over and above the one obtained by joining the incoming and outgoing arrows of the particle-particle ladder with a single-particle fermionic Green's function, as we did in Eq. (3.16). It is, however, also clear that, *by construction*, these additional terms would be of higher-order in the “low-density” parameter, and can thus be consistently neglected.

A complete numerical evaluation of Eqs. (3.11)-(3.17) exceeds the purposes of the present paper. In the next Section we shall calculate the scattering length for composite bosons in the strong-coupling limit, as a degenerate case of the T-matrix given by Eq. (3.13). This calculation will ensure us that the diagrams of Fig. 9b, be-

yond first order in the interaction potential for composite bosons, give contributions of the *same order* of magnitude as the first-order (Hartree-Fock) diagram. In addition, it will turn out that the series of diagrams depicted in Fig. 9b does *not* converge, making any truncation of the series not appropriate. For this reason, it is essential to solve the complete integral equation associated with this series of diagrams to get a correct description of the strong-coupling limit.

IV. NUMERICAL RESULTS FOR THE SCATTERING LENGTH OF COMPOSITE BOSONS

The *scattering length* a characterizes the low-energy collisions for the scattering from an ordinary potential.³⁵ For the mutual scattering of two particles (each of mass M), a can be expressed by the relation $t(0) = 4\pi a/M$ in terms of the ordinary T-matrix $t(0)$ in the limit of vanishing wave vector. In particular, within the Born approximation $t(0)$ is replaced by the Fourier transform $u(0)$ of the inter-particle potential for vanishing wave vector.

In a similar way, we shall *define* the scattering length a_B for composite bosons (each of mass $2m$) in the strong-coupling limit and for vanishing density, by setting

$$t_B(0) = \frac{4\pi}{2m} a_B \quad (4.1)$$

where $t_B(0) = (8\pi/(m^2 a_F))^2 \bar{t}_B(0)$ and $\bar{t}_B(0) \equiv \bar{t}_B(0, 0, 0, 0)$ [cf. Eqs. (2.29), (2.28), and (3.11)]. This quantity is expected to be important for the calculation of the bosonic self-energy (3.14), insofar as the generalized T-matrix for composite bosons therein depends weakly on its arguments.

To lowest order in the effective interaction for composite bosons, we can replace $t_B(0)$ by $u_2(0)$ and write

$$u_2(0) = \frac{4\pi}{2m} a_B^{\text{Born}} \quad (4.2)$$

within the Born approximation. Comparison with Eq. (2.30) yields then the value $a_B^{\text{Born}} = 2a_F$, as anticipated by Eq. (2.31). Note also that the replacement of t_B by u_2 (or, equivalently, of \bar{t}_B by \bar{u}_2) corresponds to the bosonic Hartree-Fock approximation, whereby *only* the diagram at the left in Fig. 9b is considered instead of the whole sequence.

To calculate $\bar{t}_B(0)$, it is convenient to determine first the auxiliary quantity $\bar{t}_B(q, -q, 0, 0)$ by solving the following *closed-form* equation

$$\begin{aligned} \bar{t}_B(q, -q, 0, 0) &= \bar{u}_2(q, -q, 0, 0) \\ &- \frac{1}{\beta\mathcal{V}} \sum_{q'} \bar{u}_2(q, -q, q', -q') \Gamma_o(q') \Gamma_o(-q') \bar{t}_B(q', -q', 0, 0), \end{aligned} \quad (4.3)$$

which is obtained from Eq. (3.13) by setting $q_1 = -q_2 = q$ and $q_3 = q_4 = 0$. This integral equation can be solved by

standard numerical methods, e.g., by reverting it to the solution of a system of coupled linear equations.

Before embarking into this numerical calculation, we can obtain a preliminary estimate of the value of $\bar{t}_B(0)$ with limited effort, by neglecting the four-vector dependence of \bar{t}_B as well as the frequency dependence of \bar{u}_2 on the right-hand side of Eq. (4.3). We thus write approximately:

$$\begin{aligned} \left(\frac{\bar{t}_B(0)}{\bar{u}_2(0)} \right)^{-1} &= \left(\frac{t_B(0)}{u_2(0)} \right)^{-1} \\ &\simeq 1 + \int \frac{d\mathbf{q}}{(2\pi)^3} \bar{u}_2(\mathbf{q}, -\mathbf{q}, 0, 0) \frac{1}{\beta} \sum_{\Omega_\nu} \Gamma_o(q) \Gamma_o(-q) \\ &= 1 - \int \frac{d\mathbf{q}}{(2\pi)^3} u_2(\mathbf{q}, -\mathbf{q}, 0, 0) \frac{1}{\beta} \sum_{\Omega_\nu} \frac{1}{i\Omega_\nu - \frac{q^2}{4m}} \frac{1}{i\Omega_\nu + \frac{q^2}{4m}} \\ &= 1 + \int \frac{d\mathbf{q}}{(2\pi)^3} u_2(\mathbf{q}, -\mathbf{q}, 0, 0) \frac{1}{\frac{q^2}{2m}}, \end{aligned} \quad (4.4)$$

where the last result holds to the leading order in the density. Recalling further from Ref. 16 that

$$u_2(\mathbf{q}, -\mathbf{q}, 0, 0) = u_2(0) \frac{4}{4 + (|\mathbf{q}|a_F)^2} \quad (4.5)$$

in the strong-coupling limit, we obtain for the integral on the right-hand side of Eq. (4.4) the following value (in three dimensions)

$$\int \frac{d\mathbf{q}}{(2\pi)^3} u_2(\mathbf{q}, -\mathbf{q}, 0, 0) \frac{1}{\frac{q^2}{2m}} = u_2(0) \frac{m}{\pi a_F} = 4 \quad (4.6)$$

where use has been made of the result (2.30). Comparison with Eqs. (4.1) and (4.2) yields eventually

$$\frac{a_B}{a_B^{\text{Born}}} = \frac{t_B(0)}{u_2(0)} \simeq \frac{1}{5}, \quad (4.7)$$

which implies that the contribution of the series diagrams depicted in Fig. 9b is of the *same order of magnitude* as the contribution of the first-order (Hartree-Fock) diagram therein.

The above approximate calculation suggests us to consider in more detail the scattering problem for two true bosons (each of mass M), mutually interacting via a potential of the form (4.5), namely,

$$u(\mathbf{q}) = \frac{8\pi a_F}{M} \frac{\gamma}{1 + \tilde{q}^2/4} \quad (4.8)$$

where $\tilde{q} = |\mathbf{q}|a_F$ and γ is a dimensionless coupling constant ($\gamma = 1$ and $M = 2m$ for the potential (4.5)). Solving for this simplified scattering problem will, in fact, be instructive to obtain the solution of the original scattering problem (4.3) for composite bosons, since it will (i) suggest a nontrivial approximation to be carried over to the original equation (4.3), and (ii) assess whether the region of interest ($\gamma \approx 1$) belongs to the perturbative or

nonperturbative regime of the scattering integral equation.

To this end, we recall the equation satisfied by the T-matrix for two-body scattering. In particular, it is sufficient to consider the following degenerate form

$$t(\mathbf{q}, 0) = u(\mathbf{q}) - \int \frac{d\mathbf{q}'}{(2\pi)^3} \frac{u(\mathbf{q} - \mathbf{q}') t(\mathbf{q}', 0)}{\frac{q'^2}{M}}, \quad (4.9)$$

which resembles Eq. (4.3) for composite bosons but lacks its dependence on Matsubara frequencies. As already noted, the scattering length is related to $t(0) \equiv t(0, 0)$ by the relation $a = t(0)M/(4\pi)$. For a spherically symmetric potential, $t(\mathbf{q}, 0) = t(|\mathbf{q}|, 0)$ and the angular integral in Eq. (4.9) can be readily performed. The remaining integral over $|\mathbf{q}|$ can be suitably discretized over a mesh, until convergence is achieved for the desired value $t(0)$ (200 mesh points have proved sufficient to get a 1% accuracy in the scattering length).

The results for a (in units of a_F) vs. γ are shown in Fig. 10, where the asterisks corresponds to the numerical solution of Eq. (4.9) and the full curve represents the Born approximation $a^{\text{Born}}/a_F = 2\gamma$. Note that, in the region of interest ($\gamma \approx 1$), $a^{\text{Born}}/a \approx 3$ and the solution of Eq. (4.9) cannot be obtained by perturbative methods (the perturbative region - where the Born series associated with the integral equation (4.9) for a repulsive potential would converge - is, in fact, limited by $a^{\text{Born}}/a \lesssim 2$ and corresponds to $\gamma \lesssim 0.5$). For this reason, any truncation of the integral equation would not be justified. Note also that the difference between a^{Born} and a increases drastically as γ increases (we have verified that a/a_F is proportional to $\log \gamma$ at least over eight decades).

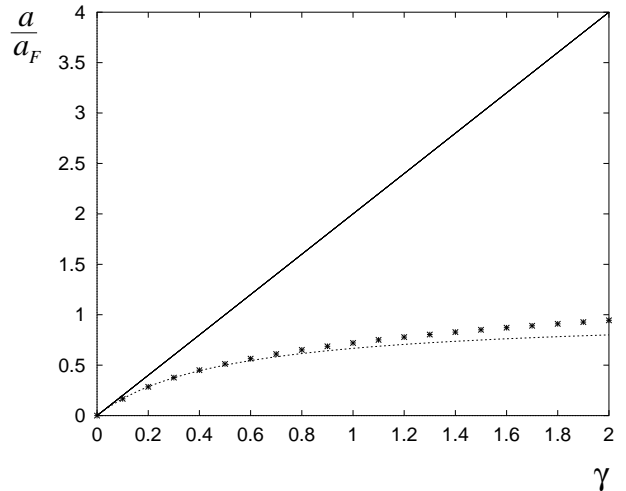


FIG. 10. Scattering length a (in units of a_F) vs. the coupling strength γ of the potential (4.8), obtained by solving numerically the integral equation (4.9) (asterisks) and by the approximate relation (4.11) (broken line). The full line represents the Born approximation $a/a_F = 2\gamma$.

Reducing the integral equation to a matrix equation

(by discretizing the integral it contains) may, however, be less accurate when solving the original equation (4.3). In that case, it might be useful to make comparison with an alternative approximate result that avoids matrix inversion altogether. The solution of the two-body problem (4.9) suggests us to get this approximate result along the following lines. Quite generally, suppose that $u(\mathbf{q})$ has a characteristic range q_o . It then follows from Eq. (4.9) that $t(\mathbf{q}, 0)$ has the *same range* q_o and is *proportional to* $u(\mathbf{q})$ for $|\mathbf{q}| \gg q_o$ (both properties can be verified by working out specific examples). Thus, if we set

$$\frac{t(\mathbf{q}, 0)}{t(0)} = \lambda(\mathbf{q}) \frac{u(\mathbf{q})}{u(0)}, \quad (4.10)$$

then $\lambda(\mathbf{q})$ varies slowly from $\lambda(0) = 1$ to $\lambda(\infty) < 1$ (for a repulsive potential). Since the integral in Eq. (4.9) weighs more “small” than “large” wave vectors, we can replace $\lambda(\mathbf{q}) \simeq \lambda(0) = 1$ therein and obtain

$$t(0) \simeq \frac{u^2(0)}{u(0) + \int \frac{d\mathbf{q}}{(2\pi)^3} \frac{u^2(\mathbf{q})}{\mathbf{q}^2/M}}. \quad (4.11)$$

The values of a/a_F obtained with this approximation are reported in Fig. 10 (broken line), and show remarkable agreement with the full numerical solution of the integral equation (4.9), from the perturbative region ($\gamma \ll 1$) up to the region of interest ($\gamma \approx 1$).

The same sort of approximation can be adopted when solving the original integral equation (4.3) for composite bosons. In this case, we set approximately

$$\frac{\bar{t}_B(q, -q, 0, 0)}{\bar{t}_B(0)} \simeq \frac{\bar{u}_2(q, -q, 0, 0)}{\bar{u}_2(0)} \quad (4.12)$$

and obtain from Eq. (4.3) the expression

$$\bar{t}_B(0) \simeq \frac{\bar{u}_2(0)^2}{\bar{u}_2(0) + \frac{1}{\beta V} \sum_q \bar{u}_2(q, -q, 0, 0)^2 \Gamma_o(q) \Gamma_o(-q)}. \quad (4.13)$$

The calculation of $\bar{u}_2(q, -q, 0, 0)$ according to the general expression (3.11) can be reduced to the numerical evaluation of an integral over $|\mathbf{k}|$, with $\mu = -\epsilon_o/2$ in the fermionic single-particle Green’s functions. The frequency part of the sum over q in Eq. (4.13) can further be reduced to an integral, since for vanishing density the range of temperature we are interested in vanishes. An accurate numerical evaluation of the ensuing integral over $|\mathbf{q}|$ and Ω in Eq. (4.13) yields

$$\frac{a_B}{a_B^{\text{Born}}} = \frac{\bar{t}_B(0)}{\bar{u}_2(0)} \simeq \frac{1}{2.69} \quad (4.14)$$

within an estimated 1% numerical accuracy.

Full numerical calculation of Eq. (4.3) requires us to introduce a finite-size mesh for the variables $(|\mathbf{q}|, \Omega)$ as

well as $(|\mathbf{q}'|, \Omega')$, with the angular integral over \hat{q}' affecting only the function $\bar{u}_2(q, -q, q', -q')$. Equation (4.3) is thus reduced to a set of coupled equations for the unknowns $\bar{t}_B(|\mathbf{q}|, \Omega; |\mathbf{q}|, -\Omega; 0, 0)$, which we have solved by the standard Newton-Raphson algorithm with a linear interpolation for the integral over $|\mathbf{q}'|$ and Ω' . In this way we obtain

$$\frac{a_B}{a_B^{\text{Born}}} = \frac{\bar{t}_B(0)}{\bar{u}_2(0)} \simeq \frac{1}{2.65} \quad (4.15)$$

within an estimated 5% numerical accuracy. The agreement between the results (4.14) and (4.15) implies that the numerical procedures we have adopted are accurate enough for the present calculation.

To verify that this result could not be inferred from a perturbative expansion of the integral equation (4.3), we calculate eventually the second term on the right-hand side of Eq. (4.3) by replacing $\bar{t}_B(q', -q', 0, 0)$ therein with $\bar{u}_2(q', -q', 0, 0)$ and by setting $q = 0$ everywhere for convenience. In this way we obtain [cf. Eq. (4.13)]:

$$\begin{aligned} \bar{t}_B(0) &\simeq \bar{u}_2(0) \left[1 - \frac{1}{\beta V} \sum_{q'} \frac{\bar{u}_2(q', -q', 0, 0)^2}{\bar{u}_2(0)} \right. \\ &\quad \left. \times \Gamma_o(q') \Gamma_o(-q') + \dots \right] \\ &= \bar{u}_2(0) (1 - 1.69 + \dots), \end{aligned} \quad (4.16)$$

showing clearly that the geometric series would not converge in this case.

To summarize, we have shown that, in the strong-coupling limit, the value $a_B = 2a_F$ obtained for the composite-boson scattering length within the self-consistent fermionic T-matrix approximation,⁹ is modified to $a_B \simeq (3/4)a_F$ by the correct inclusion of *all* low-density contributions for a system of composite bosons.

V. CONCLUDING REMARKS

In this paper, we have determined the correct diagrammatic approximation for a “dilute” system of composite bosons, which form as tightly bound pairs of fermions in the limit of strong attraction between the constituent fermions. We have emphasized that it is physically the comparison of the average interparticle distance to the characteristic length associated with the *residual* interaction between the composite bosons to determine the “diluteness” condition in the strong-coupling limit of the original fermionic attraction. For this reason, the simple argument, according to which to a “dilute” system of fermions in the weak-coupling limit there necessarily corresponds a “dilute” system of composite bosons in the strong-coupling limit, might be misleading, since two different interactions actually control the “diluteness” condition in the two limits. It is thus essential to treat the residual interaction between the composite bosons with

the due care, in order to control the strong-coupling limit of the theory appropriately. In this context, it is worth mentioning that the importance of a proper treatment of the residual boson-boson interaction in the strong-coupling limit has been emphasized in the pioneering paper by Nozières and Schmitt-Rink,³⁶ but never duly taken into account in subsequent work.

We have also shown that the selection of the diagrammatic contributions according to the “diluteness” parameter proceeds along quite different lines in the weak-coupling limit (where the small parameter is $k_F a_F$) and in the strong-coupling limit (where the small parameter is $\rho_B^{1/3} a_B$).¹⁴ Accordingly, diagrammatic contributions of the *same* order in $\rho_B^{1/3} a_B$ in the strong-coupling limit correspond, in general, to *different* powers of $k_F a_F$ in the weak-coupling limit. Mathematically, this difference is due to the behaviour of the fermionic particle-particle ladder, which reduces to a constant in the weak-coupling limit but develops a singularity in the strong-coupling limit.

Our selection of diagrammatic contributions has rested on a suitable regularization of the fermionic interaction, which has caused the ratio between the particle-particle and particle-hole contributions to be infinite. For a Hubbard Hamiltonian on a lattice, where this regularization cannot be applied, we expect the difference between p-p and p-h contributions to be less extreme albeit still appreciable, so that our selection of diagrammatic contributions may still remain valid.³⁷

Quite generally, we have remarked that, with our choice of the fermionic interaction, the most general structure of the diagrammatic theory is constructed with the “bare” particle-particle ladder plus an infinite set of (four, six, \dots , -point) vertices. This remains true for *any* value of the fermionic coupling and not just in the strong-coupling limit where the composite bosons form. We have also remarked that the “diluteness” parameter ($k_F a_F$ or $\rho_B^{1/3} a_B$) emerges *naturally* from the theory, both in the weak- and strong-coupling limits, without having to be imposed as an external condition. Accordingly, keeping tracks of the powers of this small parameter in the diagrammatic theory can be relevant *only* in the weak- and strong-coupling limits. In the intermediate-coupling (crossover) region, on the other hand, a small parameter is lacking and consequently the diagrammatic approximations cannot be controlled by any means.³⁸

For these reasons, implementing the self-consistency of the fermionic Green’s functions within the fermionic T-matrix approximation does not seem *a priori* to be an important issue for the BCS-BE crossover. Self-consistency, in fact, drops out in the weak- and strong-coupling limits when the “diluteness” parameter is small, while in the intermediate (crossover) region inclusion of self-consistency within the fermionic T-matrix approximation (as well as within any other approximation over and above it) *cannot anyway be controlled* by the lack of a small parameter (even though inclusion of self-consistency might produce

in practice sizable numerical effects).

We have emphasized in this paper that the (self-consistent) fermionic T-matrix approximation does not account properly for the boson-boson interaction in the strong-coupling limit, at least in *three* dimensions. This approximation, however, has been recently adopted to discuss pseudo-gap and related issues within the negative- U Hubbard model in *two* dimensions.^{39–41} Assessing to what extent the approach we have developed in this paper can be carried over to the two-dimensional case is not *a priori* evident and will require further investigations. From physical intuition one would expect the bosonic regime to be reached even more effectively in two than in three dimensions, insofar as the two-fermion bound state is present in two dimensions for any (attractive) coupling strength.⁴² Our dealing with the three-dimensional case first was required for manifesting at the outset the effects on the BCS-BE crossover due to the progressive formation of bound-fermion pairs, thus isolating them from other effects which are peculiar to the two-dimensional case.

We have considered in this paper temperatures *above* T_c only. Extending our approach below T_c even for the three-dimensional case will also require further investigations. In fact, divergencies occur in the particle-particle channel when approaching the critical temperature,²⁷ over and above the divergencies due to the formation of a bound state in the associated two-body problem, which we have taken care of in this paper.

It is interesting to point out that, when written in terms of the constituent fermions (cf. Fig. 13 below), the diagrammatic structure introduced by our approach bears some analogy with the parquet approximation utilized for the positive- U Hubbard model.⁵ In addition, the level of numerical effort required to solve our integral equation Eq. (3.13) for the generalized T-matrix for composite bosons appears to be comparable with the effort required to solve the integral equations defining the parquet scheme.⁴³

It is also interesting to point out the strong analogy between the present treatment of the BCS to BE crossover in a condensed matter system and the so-called OAI mapping introduced some time ago in nuclear physics,^{44,45} where a systematic mapping between the diagrammatic theories for (composite) bosons and (constituent) fermions is also provided, albeit in a quite different physical context and with the use of approximations more specific to the nuclear problem.

A final comment is in order about the emphasis we have given to the correct description of the boson-boson interaction in the strong-coupling limit. We know, in fact, that in the *extreme* strong-coupling limit the boson-boson interaction can be neglected and the composite bosons become effectively free. Since this extreme limit of free composite bosons is also retrieved by the (self-consistent) fermionic T-matrix approximation, it would appear that the improvement brought about by our theory (which takes specifically into account the interaction

between the composite bosons) affects only *the way this extreme limit is approached*. That the important physics may reside in the correct description of the *approach* to the asymptotic regimes and not merely of the asymptotic regimes themselves, can be confirmed from previous experience with the so-called Hubbard-III solution;⁴⁶ in that case, neither the weakly-interacting (Fermi liquid) nor the strongly-interacting (Kondo) physics is reproduced, although the extreme (non-interacting and atomic) limits are both retrieved.

ACKNOWLEDGMENTS

We are indebted to C. Castellani, C. Di Castro, M. Grilli, F. Iachello, V. Janiš, A. Perali, and F. Pistolesi for helpful discussions. One of us (P.P.) gratefully acknowledges receipt of a postdoctoral research fellowship from the Italian INFN under contract PRA-HTCS/96-98.

APPENDIX A: COMPOSITE-BOSON PROPAGATOR AND TWO-FERMION GREEN'S FUNCTION

It was shown in Ref. 16 (cf. Appendix A therein) that the average value of $b(q=0)$ (taken with the effective bosonic action (2.19)) is proportional to the average value of the operator (2.16) (taken with the original fermionic action (2.15)). Purpose of this Appendix is to show that a similar relation holds between the “full” bosonic propagator $\langle b^*(q)b(q) \rangle_{S_{\text{eff}}}$ and the average value of the product of two operators (2.16).

To this end, it is convenient to add to the original fermionic action (2.15) the following (source) term

$$\delta S = \int_0^\beta d\tau \sum_{\mathbf{q}} [J(\mathbf{q}, \tau) \bar{\mathcal{B}}(\mathbf{q}, \tau) + J^*(\mathbf{q}, \tau) \mathcal{B}(\mathbf{q}, \tau)] \quad (\text{A1})$$

and to define the fermionic generating functional [cf. Eq. (2.14)]

$$\mathcal{Z}[J, J^*] = \frac{\int \mathcal{D}\bar{c}\mathcal{D}c \exp\{-S - \delta S\}}{\int \mathcal{D}\bar{c}\mathcal{D}c \exp\{-S\}}. \quad (\text{A2})$$

Introducing the Hubbard-Stratonovich transformation (2.17), shifting the bosonic integration variables by letting $b(\mathbf{q}, \tau) \rightarrow b(\mathbf{q}, \tau) + J(\mathbf{q}, \tau)$, and integrating out the Grassmann variables, we obtain the exact identity:

$$\left. \frac{\delta \mathcal{Z}[J, J^*]}{\delta J(\mathbf{q}, \tau') \delta J^*(\mathbf{q}, \tau)} \right|_{J=J^*=0} = \frac{1}{V^2} \langle b^*(\mathbf{q}, \tau') b(\mathbf{q}, \tau) \rangle_{S_{\text{eff}}} + \frac{1}{V} \delta(\tau - \tau'). \quad (\text{A3})$$

Upon differentiating the original expression (A2) in a similar way and comparing with Eq. (A3), we obtain eventually the desired relation:

$$\langle b^*(\mathbf{q}, \tau') b(\mathbf{q}, \tau) \rangle_{S_{\text{eff}}} = V^2 \langle \bar{\mathcal{B}}(\mathbf{q}, \tau') \mathcal{B}(\mathbf{q}, \tau) \rangle_S - V \delta(\tau - \tau'), \quad (\text{A4})$$

where the last term on the right-hand side can be dropped since it vanishes with the regularization (2.4) in the limit $k_o \rightarrow \infty$.

The result (A4) can be conveniently interpreted in diagrammatic terms as follows. Taking the Matsubara Fourier transform of both sides of Eq. (A4) yields

$$\begin{aligned} \langle b^*(q)b(q) \rangle_{S_{\text{eff}}} &= V^2 \sum_{k, k'} w(\mathbf{k} + \mathbf{q}/2) w(\mathbf{k}' + \mathbf{q}/2) \\ &\times \langle \bar{c}_\uparrow(k+q) \bar{c}_\downarrow(-k) c_\downarrow(-k') c_\uparrow(k'+q) \rangle_S \\ &\equiv V^2 \sum_{k, k'} w(\mathbf{k} + \mathbf{q}/2) w(\mathbf{k}' + \mathbf{q}/2) \mathcal{G}_2(k, k'; q) \end{aligned} \quad (\text{A5})$$

which defines the fermionic two-particle Green's function \mathcal{G}_2 in the particle-particle channel. This function is depicted in Fig. 11, in terms of the single-particle fermionic Green's functions \mathcal{G} and of the generalized particle-particle ladder Γ . Note that the external single-particle lines of Fig. 11 (as well as the single-particle lines contained in Γ) include, in principle, self-energy insertions.

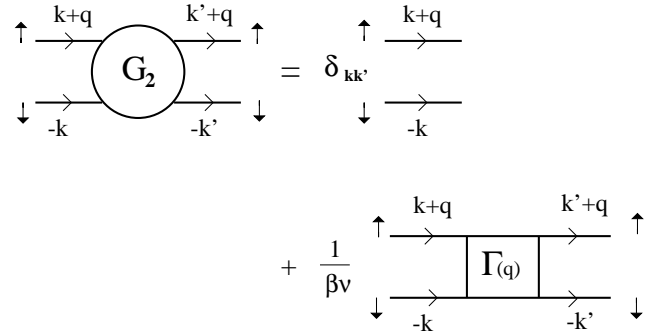


FIG. 11. Fermionic two-particle Green's function \mathcal{G}_2 , expressed in terms of the “full” single-particle Green's function \mathcal{G} (represented here by a line) and of the generalized particle-particle ladder Γ (represented by a box). The factor $(\beta V)^{-1}$ originates from the diagrammatic rules. Spin labels are indicated by up and down arrows.

Owing to our choice of a “contact” potential, the generalized particle-particle ladder of Fig. 11 depends only on the sum q of the incoming (outgoing) four-momenta. For this reason, the sums over k and k' in Eq. (A5) are decoupled and affect only the external single-particle lines. Let

$$\mathcal{I}_{pp}(q) = \frac{V}{\beta} \sum_k w(\mathbf{k} + \mathbf{q}/2) \mathcal{G}(k+q) \mathcal{G}(-k) \quad (\text{A6})$$

be the analogue of the quantity $\mathcal{I}_{pp}(q)$ introduced in Eq. (2.5), where now the full single-particle fermionic

Green's function \mathcal{G} replaces its bare counterpart \mathcal{G}^o . We know already that $I_{pp} = -1 + \mathcal{O}(k_o^{-1})$, whereby only the behavior of \mathcal{G}^o for large wave vectors contributes to the finite term. The self-energy insertions contained in \mathcal{G} cannot modify this result, since they vanish for large wave vectors (provided a well-defined *finite* expression is associated with the self-energy itself in the limit $k_o \rightarrow \infty$). This remark implies that also $\mathcal{I}_{pp} = -1 + \mathcal{O}(k_o^{-1})$.

Combining Eq. (A5) with the representation of Fig. 11, we then obtain the following relation between the “full” bosonic propagator and the generalized particle-particle ladder:

$$\langle b^*(q)b(q) \rangle_{S_{\text{eff}}} = \frac{\beta}{V} \Gamma(q) \quad (\text{A7})$$

of which Eq. (2.26) of the text is the simplest approximation. It is clear from our derivation that the result (A7) holds irrespective of the value of the fermionic scattering length a_F .

The equivalence (A7) between the generalized particle-particle ladder and the “full” bosonic propagator is basic to the purposes of the present paper, since it enables us to interpret in a rigorous fashion the general diagrammatic structure of $\Gamma(q)$ in terms of the building blocks of the diagrammatic structure of $\langle b^*(q)b(q) \rangle_{S_{\text{eff}}}$, namely, the “bare” bosonic propagator $\langle b^*(q)b(q) \rangle_{S_{\text{eff}}^2}$ given by Eq. (2.26) and the four, six, \dots , n -point interaction vertices given by Eqs. (2.28), (2.33), \dots , in the order.

APPENDIX B: FERMIONIC DIAGRAMS CORRESPONDING TO THE T-MATRIX APPROXIMATION FOR COMPOSITE BOSONS

In this Appendix we discuss the mapping between the diagrammatic structures of the composite bosons and the constituent fermions, for the case when only the four-point interaction vertex for composite bosons is retained and all higher-order vertices are neglected. In particular, we shall consider the class of diagrams of interest depicted in Fig. 9b, corresponding to the T-matrix approximation for composite bosons. To make our argument more complete, we shall also consider one additional bosonic diagram not belonging to this class, owing to its peculiar topological structure. By working out these two examples in detail, we shall establish a definite correspondence between the value of the symmetry factors for the bosonic diagrammatic structure and the number of independent diagrams in the associated fermionic structure, as anticipated in the Introduction. Besides providing a compelling check on the general structure of our mapping, determining the *explicit form* of the fermionic diagrams proves useful to verify that our generalized T-matrix approximation correctly reduces to the standard fermionic (Galitskii) approximation in the weak-coupling limit.

We begin by determining the symmetry factors associated with the diagrams of Fig. 8b for true bosons,

where the two-body interaction is assumed to be suitably symmetrized. The symmetry factor \mathcal{S}_L associated with the diagram containing L interaction vertices is given by the ratio of the number of ways to construct this diagram from the corresponding prediagram and the factor $4^L L!$ originating from the perturbative expansion at order L .^{20,21} By definition, in the prediagram only the external (incoming and outgoing) arrows of the self-energy and the interaction vertices appear, but not the propagators that join the vertices among themselves or with the external arrows. Note that, for a complex bosonic field, the interaction vertices bear directional arrows and, consequently, the number of ways to join them with the propagators differs from the value of the standard ϕ^4 theory with a real field. One can readily show that the number of ways to construct the diagram of Fig. 8b with L interaction vertices from the corresponding prediagram is given by $2^{L+1} L!$, yielding for the symmetry factor the value

$$\mathcal{S}_L = \frac{2^{L+1} L!}{4^L L!} = \frac{1}{2^{L-1}}. \quad (\text{B1})$$

Since for this set of diagrams all arrangements of vertices and propagators produce different contractions (according to Wick's theorem), no other factor is required in this case beside the symmetry factor (B1).⁴⁷

It is clear that with the diagrams of Fig. 9b for composite bosons is also associated the *same* symmetry factor (B1), as they share the same topological structure of the diagrams of Fig. 8b. Since the symmetry factor of any fermionic diagram is instead bound to be unity,³¹ we expect \mathcal{S}_L^{-1} *identical* fermionic diagrams to be associated with a given diagram for composite bosons having symmetry factor \mathcal{S}_L .

To verify this statement, we recall the correspondence (shown in Fig. 4) of the propagator and vertex of the bosonic theory with the building blocks of the fermionic diagrammatic structure (which takes also into account the spin labels). In subsection IIB we have already discussed the case with $L = 1$ and $\mathcal{S}_1 = 1$, with which two distinct fermionic diagrams have consistently been associated (cf. Fig. 5). The case with $L = 2$ and $\mathcal{S}_2 = 1/2$ is shown graphically in Fig. 12. In this case, it can be readily verified that the four possible fermionic diagrams (obtained by associating *two* distinct fermionic structures to each bosonic vertex via the rules of Fig. 4b) are equal in pairs. The resulting factor of 2 multiplying each independent fermionic diagram is then canceled by the symmetry factor $\mathcal{S}_2 = 1/2$, so that each independent fermionic diagram is correctly multiplied by unity, as anticipated.

By a similar token, when $L = 3$ one can verify that, out of the eight possible fermionic diagrams, only two are independent. The ensuing factor of 4 in front of each of these two independent diagrams is then canceled by the symmetry factor $\mathcal{S}_3 = 1/4$. More generally, if we call “up” and “down”, respectively, the two fermionic structures associated in Fig. 4b with the bosonic four-point vertex, it can be verified that fermionic diagrams,

obtained from each other by replacing a *pair* of “up” by a pair of “down” fermionic structures, are equal. This property is *sufficient* to guarantee that each distinct fermionic diagram is correctly multiplied by unity. Consider, for instance, two nontrivial cases with odd ($L = 5$) and even ($L = 6$) number of bosonic vertices. When $L = 5$, $2^5 = 32$ fermionic diagrams are generated from the bosonic diagram. In this case, from the single fermionic diagram with all “up” structures we can generate $5!/(3!2!)=10$ diagrams with three “up” and two “down” structures, and $5!/(1!4!)=5$ diagrams with one “up” and four “down” structures, for a total of $1+10+5=16$ identical fermionic diagrams. The same number of identical diagrams results from the other independent diagram having all “down” structures (which, evidently, cannot be obtained from the previous diagram with all “up” structures by replacing an even number of “up” structures by “down” structures). The resulting factor of 16 associated with each of these two independent fermionic diagrams is then canceled by the symmetry factor $\mathcal{S}_5 = 1/16$, and each independent fermionic diagram is correctly multiplied by unity.

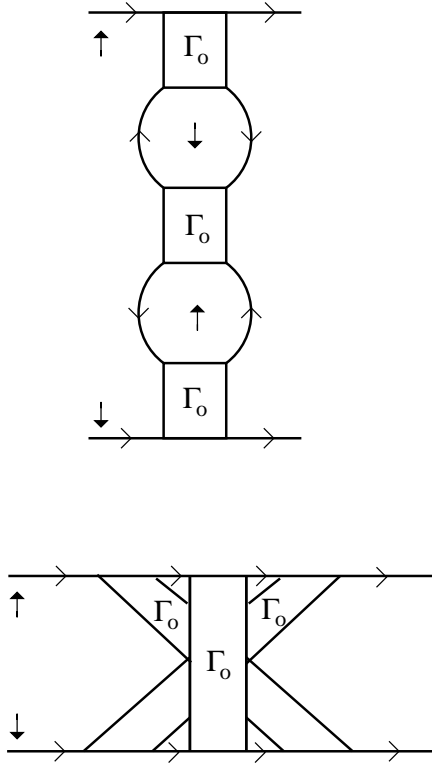


FIG. 12. The two distinct fermionic diagrams corresponding to the bosonic diagram with two interaction vertices ($L = 2$ and $\mathcal{S}_2 = 1/2$) depicted in Fig. 9b. Boxes and full lines stand for the “bare” particle-particle ladder Γ_o and for the “bare” single-particle fermionic Green’s function \mathcal{G}^o , respectively.

When $L = 6$, $2^6 = 64$ fermionic diagrams are generated from the bosonic diagram. In this case, the two

independent diagrams (out of the 64 possible fermionic diagrams) have either all “up” structures or five “up” and one “down” structures. To the first case we associate $1+6!/(4!2!)+6!/(2!4!)+1=32$ identical diagrams, and to the second case $6!/(5!1!)+6!/(3!3!)+6!/(1!5!)=32$ identical diagrams. The resulting factor of 32 multiplying each independent fermionic diagram is then canceled by the symmetry factor $\mathcal{S}_6 = 1/32$, and each independent fermionic diagram is again correctly multiplied by unity.

Quite generally, one can show that the fermionic diagrams associated with the T-matrix diagrams of Fig. 9b for composite bosons can be organized into *three classes*, containing zero, one, and two fermionic loops, respectively. A representative diagram of each of these three classes is depicted in Fig. 13a, Fig. 13b, and Fig. 13c, in the order. Note that fermionic diagrams containing zero or two loops are associated with bosonic diagrams with an *even* number of interaction vertices, while fermionic diagrams containing one loop are associated with bosonic diagrams with an *odd* number of interaction vertices (cf. the comment made in subsection IIB while discussing Fig. 5).

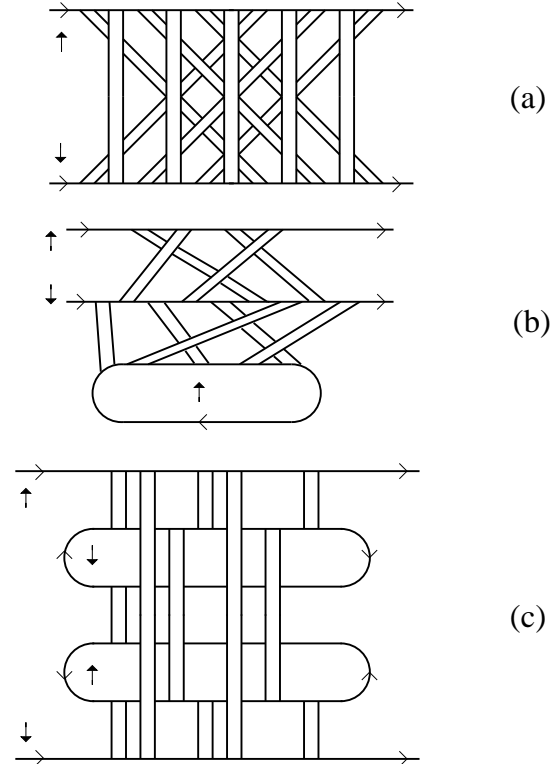


FIG. 13. Representative diagrams of the three classes of fermionic diagrams associated with the bosonic T-matrix, containing (a) zero, (b) one, and (c) two fermionic loops. Conventions are as in Fig. 12.

The above analysis can be made more systematic, by allowing also for the possibility of “twisting” pairs of fermionic lines while connecting the fermionic particle-

particle ladder of Fig. 4a with the four-point vertex of Fig. 4b. In other words, one may consider the situation where two pairs of fermionic lines, which would not be allowed to connect with each other “directly” as their spins would not match, are instead allowed to connect by “twisting” one pair of lines with respect to the other one. A careful analysis of the unraveling of the fermionic diagrams containing “twistings”, however, shows that no new diagram is introduced in this way, over and above the diagrams depicted in Fig. 13 which have been generated by not allowing “twisted” connections.

We are now in a position to verify that the fermionic diagrams, associated with the generalized T-matrix approximation for composite bosons, correctly reduce to the standard Galitskii approximation in the weak-coupling limit, in the sense that they yield contributions of progressively higher order in the small parameter $k_F a_F$ with respect to the “bare” particle-particle ladder. For instance, while the particle-particle ladder is proportional to a_F in the weak-coupling limit (cf. Eq. (2.10)), corrections to this ladder due to the simple diagrams of Fig. 5 are readily seen to be smaller by a factor $(k_F a_F)^2$. Similarly, corrections to the particle-particle ladder due to the diagrams of Fig. 12 are smaller by a factor $(k_F a_F)^4$ with respect to the “bare” ladder. In general, to estimate in the weak-coupling limit the order in $k_F a_F$ of a given diagram contributing to the generalized particle-particle ladder Γ , we can rely on *dimensional considerations*, by counting the powers of a_F in terms of the number of “bare” ladders Γ_o and the powers of k_F in terms of the dimensionality of the four-vector sums over products of internal single-particle fermionic Green’s functions (which can safely be done because all sums are convergent). By this procedure, we obtain that, in the weak-coupling limit, the diagram of order L within the bosonic T-matrix approximation is smaller by a factor $(k_F a_F)^{2L}$ with respect to the “bare” ladder Γ_o .

This proves that diagrams of the same order in $\rho_B^{1/3} a_B$ in the bosonic (strong-coupling) limit end up having *different* orders in $k_F a_F$ in the fermionic (weak-coupling) limit; accordingly, they would have been dismissed as being irrelevant, if the selection of diagrams would have been made directly for the weak-coupling limit.

Finally, let us consider the bosonic diagram of Fig. 14 which does not belong to the set of T-matrix diagrams. For this diagram, a naive counting of the number of ways it can be constructed from the corresponding prediagram would give unity for the symmetry factor. However, a more careful analysis shows that a permutation of the two internal vertices is actually equivalent to a renaming the propagators joining these vertices, and has thus not to be regarded as an independent permutation.⁴⁷ This implies that the bosonic symmetry factor for the diagram of Fig. 14 is 1/2 and not 1. As a matter of fact, when generating the fermionic diagrams associated with this bosonic diagram according to the correspondence rules of Fig. 4, one finds that the $2^4 = 16$ diagrams (produced

by the presence of four bosonic interaction vertices) are equal in pairs, yielding just 8 distinct fermionic diagrams in agreement with the value 1/2 of the bosonic symmetry factor. As before, this result is not affected by introducing “twistings”.

Although we have examined in detail only two kinds of bosonic diagrams, we expect the correspondence between the bosonic symmetry factor and the number of independent fermionic diagrams to remain valid for all possible diagrams.

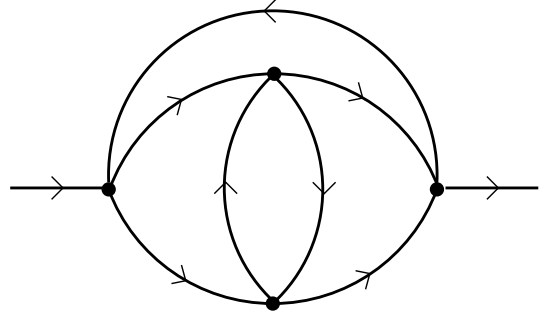


FIG. 14. Bosonic diagram with four interaction vertices, which does not belong to the set of T-matrix diagrams and possesses a special internal symmetry.

-
- ¹ Y.J. Uemura *et al.*, Phys. Rev. Lett. **62**, 2317 (1989).
 - ² H. Ding *et al.*, Nature **382**, 51 (1996); and Phys. Rev. Lett. **78**, 2628 (1997).
 - ³ A.G. Loeser *et al.*, Science **273**, 325 (1996).
 - ⁴ M.R. Norman, H. Ding, M. Randeria, and J.C. Cam-puzano, Cond-Mat./9710185.
 - ⁵ V. Janiš, J. Phys. Condens. Matter **10**, 2915 (1998).
 - ⁶ V.M. Galitskii, Sov. Phys.-JETP **7**, 104 (1958).
 - ⁷ S.T. Beliaev, Sov. Phys.-JETP **7**, 299 (1958).
 - ⁸ R. Frésard, B. Glaser, and P. Wölfle, J. Phys. Condens. Matter **4**, 8565 (1992).
 - ⁹ R. Haussmann, Z. Phys. B **91**, 291 (1993).
 - ¹⁰ R. Micnas *et al.*, Phys. Rev. B **52**, 16223 (1995).
 - ¹¹ B. Jankó, J. Maly, and K. Levin, Phys. Rev. B **56**, R11407 (1997).
 - ¹² J.R. Engelbrecht, A. Nazarenko, M. Randeria, and E. Dagotto, Phys. Rev. B **57**, 13406 (1998).
 - ¹³ B. Kyung, E.G. Klepfish, and P.E. Kornilovitch, Phys. Rev. Lett. **80**, 3109 (1998).
 - ¹⁴ In the *extreme* strong-coupling limit, the interaction between the composite bosons is bound to vanish (cf.^{9,16}). Physically, this is due to the fact that, for a point-contact interaction between the constituent fermions, the composite bosons of size a_F mutually interact only when overlapping. For this reason, the bosonic scattering length a_B should be proportional to a_F . The condition $k_F a_F \ll 1$ can then be interpreted as $\rho_B^{1/3} a_B \ll 1$, which is the “di-

luteness” condition for a Bose gas. The “diluteness” condition thus emerges naturally both in the weak- and strong-coupling limits, and should *not* be imposed as an additional condition on the system.

- ¹⁵ C.A.R. Sá de Melo, M. Randeria, and J.R. Engelbrecht, Phys. Rev. Lett. **71**, 3202 (1993).
- ¹⁶ F. Pistolesi and G.C. Strinati, Phys. Rev. **B53**, 15168 (1996).
- ¹⁷ S. Stintzing and W. Zwerger, Phys. Rev. **B56**, 9004 (1997).
- ¹⁸ Already at the mean-field level, the exact solution available for a contact potential (M. Marini, F. Pistolesi, and G.C. Strinati, Eur. Phys. J. **B1**, 151 (1998)) shows that approximations valid on the BE side extrapolate well to the BCS side, but not viceversa.
- ¹⁹ Throughout this paper, by bosonic Hartree-Fock approximation we shall mean the self-energy diagram of lowest order in the (symmetrized) bosonic interaction, that has the *same* topological structure of the bosonic Hartree-Fock self-energy diagram but lacks the self-consistency in the bosonic propagator.
- ²⁰ V.N. Popov, *Functional Integrals in Quantum Field Theory and Statistical Physics* (Riedel, Dordrecht, 1983).
- ²¹ V.N. Popov, *Functional Integrals and Collective Excitations* (Cambridge University Press, Cambridge, 1987).
- ²² G. Baym and L.P. Kadanoff, Phys. Rev. **124**, 287 (1961).
- ²³ G. Baym, Phys. Rev. **127**, 1391 (1962).
- ²⁴ In principle, by this procedure one should complement the chosen set of two-fermion diagrams with all companion diagrams, as prescribed by the Baym-Kadanoff method. In practice, however, these additional diagrams will not be included in our theory since they are of higher order in the “gas parameter” $\rho_B^{1/3} a_B$. This point will be discussed further in Section III.
- ²⁵ The choice of the “contact” potential (2.2) does not allow the fermionic attraction to extend over a *finite* range. If a finite-range fermionic attraction would instead be adopted, the effective boson-boson potential in the strong-coupling limit would acquire an *attractive* part which would dominate over the usual repulsive part due to Pauli principle, in the sense that the bosonic scattering length associated with the attractive part would not vanish in that limit. The attractive part would thus lead to an instability of the bosonic system when the finite-range fermionic attraction gets sufficiently strong. To avoid this instability, a condition of the type $\epsilon_o \ll k_o^2/(2m)$ has to be imposed on the BE limit, where k_o is the wave vector specifying the finite range of the potential [cf. footnote 43 of Ref. 16]. In this context, it is worth mentioning the recent work by G. Röpke *et al.* [Phys. Rev. Lett. **80**, 3177 (1998)] where it has been shown that, in the strong-coupling limit, there exists a competition between pair and quartet condensation in a Fermi liquid with finite-range attraction. It is then clear that adopting a finite-range fermionic potential merely makes the BCS-BE crossover more involved, and it is thus not relevant to the purposes of the present paper.
- ²⁶ It is interesting to point out that the set of diagrams defining the so-called FLEX approximation to the fermionic self-energy [cf. N.E. Bickers and D.J. Scalapino, Ann. Phys. **193**, 206 (1989)] reduces to the set of diagrams associated with the self-consistent T-matrix approximation, when the

fermionic interaction potential is regularized according to the prescription (2.4).

- ²⁷ A precise definition of what is meant by “weak-” and “strong-” coupling limits is in order at this point. In the weak-coupling limit, we let a_F vanish while keeping the density ρ and the temperature T *finite*. In this way, the terms within parentheses in Eq. (2.10) proportional to $k_F a_F$ and $k_\alpha a_F$ are negligible with respect to unity as $a_F \rightarrow 0$. Otherwise, if one would keep T close to the BCS critical temperature T_c^{BCS} as $a_F \rightarrow 0$, the terms within parentheses in Eq. (2.10) proportional to $k_F a_F$ and $k_\alpha a_F$ would no longer be negligible, since they would become proportional to $\ln(k_F^2/mT)$, and consequently the left-hand side of Eq. (2.10) would diverge as $T \rightarrow T_c^{BCS}$. In the strong-coupling limit, on the other hand we let the binding energy ϵ_o of the two-body bound state go to infinity, for given values of ρ and T . For vanishing ρ , we expect the chemical potential to approach $-\epsilon_o/2$ on physical grounds. Corrections to this value due to finite density and temperature effects are further expected to be negligible, provided $\rho^{2/3}/(2m) \ll \epsilon_o$ and $T \ll \epsilon_o$. Both conditions are met when $\epsilon_o \rightarrow \infty$, yielding $\beta\mu \rightarrow -\infty$ in the strong-coupling limit.
- ²⁸ S. Hikami, Phys. Rev. **B24**, 2671 (1981).
- ²⁹ Note that $u_2(0)$ is *positive* in the strong-coupling limit, thus ensuring the *stability* of the bosonic system. It turns out that higher-order vertices $u_l(0)$ with $l \geq 3$ are also positive, because the minus sign occurring in the definition of the vertices with odd values of l (cf. Eq. (2.33) for $l = 3$) is compensated by the presence of an appropriate number of factors $\sqrt{D(0)}$, as in Eq. (3.6) below.
- ³⁰ It can be readily verified that, if at least one $(2l)$ -point vertex enters a bosonic self-energy diagram, then there are at least $(l - 1)$ bosonic cycles in that diagram (see also Ref. 33). Since each bosonic cycle gives a contribution proportional to the density ρ (as shown in Section III), four-point vertices only contribute to the bosonic self-energy to lowest order in ρ .
- ³¹ Cf., e.g., A.L. Fetter and J.D. Walecka, *Quantum Theory of Many-Particle Systems* (McGraw-Hill, New York, 1971).
- ³² Self-consistency gives contributions at least of order $(k_F a_F)^2$ to the fermionic self-energy. For this reason, it was not considered by Galitskii in the calculation of the self-energy to order $k_F a_F$. A first round of self-consistency was, however, included by Galitskii in the calculation of the self-energy of a “dilute” Fermi gas to order $(k_F a_F)^2$.⁶ In the context of the BCS-BE crossover, the complete self-consistency within the fermionic T-matrix approximation has been considered only recently (cf. Refs. 8 and 9), and since then utilized by several authors in this field.^{10,12,13}
- ³³ In the context of the “dilute” Bose gas the term “cycle” has a specific meaning, different from the term “loop” utilized in Field Theory in the context of the loop expansion.²¹ By a “cycle” we mean, in fact, a sequence of bosonic propagators arranged in a closed path, with *all arrows running in the same direction* and with a common four-momentum integration for all propagators.
- ³⁴ The factor $D(q)$ entering Eq. (3.4) reflects the existence of the “internal” wave function φ for the composite bosons. In fact, if one defines the composite-boson field operator

$$\Psi_B(\mathbf{r}) = \int d\rho \psi_\downarrow(\mathbf{r} - \rho/2) \psi_\uparrow(\mathbf{r} + \rho/2) \varphi(\rho)$$

in terms of the field operator ψ_σ of the constituent fermions and of the “internal” wave function (which in wave vector representation reads $\varphi(\mathbf{k}) = (8\pi/a_F)^{1/2} (\mathbf{k}^2 + a_F^{-2})^{-1}$), one obtains for the composite-boson Green’s function in the strong-coupling limit:

$$\begin{aligned} \mathcal{G}_B(q) &= - \frac{2}{1 + \sqrt{1 + (-i\Omega_\nu + \mathbf{q}^2/(4m) - \mu_B)/\epsilon_o}} \frac{\beta}{\mathcal{V}} \frac{\Gamma_o}{D(q)} \\ &\equiv \frac{-1}{i\Omega_\nu - \mathbf{q}^2/(4m) + \mu_B} \end{aligned}$$

with $D(q)$ given by Eq. (3.5). Owing to the definition (2.26) and provided the condition $|i\Omega_\nu - \mathbf{q}^2/(4m) + \mu_B| \ll \epsilon_o$ is satisfied, one recovers eventually the expression (3.4) for $\langle b^*(q)b(q) \rangle_{S_{\text{eff}}^{(2)}}$. Note that the above condition corresponds to the “internal” degrees of freedom of the composite bosons not being excited.

³⁵ E. Fermi, *Nuovo Cimento* **11**, 157 (1934).

³⁶ P. Nozières and S. Schmitt-Rink, *J. Low. Temp. Phys.* **59**, 195 (1985).

³⁷ A. Perali, private communication.

³⁸ In the intermediate (crossover) region one may compare diagrammatic calculations with non-perturbative results, obtained, e.g., by a Quantum Monte Carlo approach. In this context, we mention the work by N. Trivedi and M. Randeria [*Phys. Rev. Lett.* **75**, 312 (1995)] and by J.M. Singer *et al.* [*Phys. Rev. B* **54**, 1286 (1996)] for the negative- U Hubbard model.

³⁹ J.J. Deisz, D.W. Hess, and J.W. Serene, *Phys. Rev. Lett.* **80**, 373 (1998).

⁴⁰ J.R. Engelbrecht and A. Nazarenko, *Cond-Mat./9806223*.

⁴¹ P.E. Kornilovitch and B. Kyung, *Cond-Mat./9808107*.

⁴² M. Randeria, Ji-Min Duan, and Lih-Yir Shieh, *Phys. Rev. Lett.* **62**, 981 (1989).

⁴³ V. Janiš, in *Proceedings of the International Workshop on Electron Correlations and Material Properties*, Crete (Greece), edited by N. Kioussis and A. Gonis (Plenum Press, 1998).

⁴⁴ T. Otsuka, A. Arima, and F. Iachello, *Nucl. Phys.* **A309**, 1 (1978).

⁴⁵ F. Iachello and I. Talmi, *Rev. Mod. Phys.* **59**, 339 (1987).

⁴⁶ J. Hubbard, *Proc. Roy. Soc. (London)* **A281**, 401 (1964); see also G. Czycholl, *Phys. Rep.* **143**, 277 (1986) (we are indebted with V. Janiš for bringing this reference to our attention).

⁴⁷ Cf., e.g., J.J. Binney, N.J. Dowrick, A.J. Fisher, and M.E.J. Newman, *The Theory of Critical Phenomena* (Clarendon Press, Oxford, 1993), Chapt.8.